

https://dspace.org/

Investigation of the release of gaseous fission products from pebble bed molecular reactor's triso coated fuel particle during the HFR-K5 fuel irradiation test

Leotlela, Moebetsi J.

2010-09-07
http://hdl.handle.net/10539/8618

Downloaded from a DSpace repository. https://dspace.org/

INVESTIGATION OF THE RELEASE OF GASEOUS FISSION PRODUCTS FROM PEBBLE BED MODULAR REACTOR'S TRISO COATED FUEL PARTICLE DURING THE HFR-K5 FUEL IRRADIATION TEST

Mosebetsi J Leotlela

A Research Report submitted to the Faculty of Science,
University of the Witwatersrand, Johannesburg,
in partial fulfilment
of the requirements for the degree of
Master of Science.

Johannesburg, 2010

DECLARATION

I declare that this Research Report is my own, unaided work. It is being submitted for the degree of Master of Science in the University of the Witwatersrand, Johannesburg. It has not been submitted before for any degree or examination in any University

…….

MJ Leotlela

…….day of ……2010

ABSTRACT

The effectiveness of the Tri-isotropic (TRISO) fuel particle to perform as an effective barrier to fission product migration and retain all fission products within the fuel particle is based primarily on the ability of the silicon carbide (SiC) layer to maintain its integrity in spite of the operating conditions of the Pebble Bed Modular Reactor (PBMR). However, because of the complexity of the fission product migration phenomena, fission products continue to escape through the fuel barriers in spite all efforts having being done to confine them within the fuel kernel. This suggests that there is still a lot of work still to be done to understand fission gas migration phenomena, which is the subject of this Research Report. This Research Report will concentrate on the analysis of the gaseous fission products released during the HFR-K5 fuel test, as part of the validation of the PBMR gaseous fission product release calculation model.

Investigations done on similar fuel by other researchers suggests that some of the most important factors that determine the rate of fission product migration are irradiation temperature, neutron fluence, the diffusion mechanism i.e. vacancy as opposed to interstitial mechanism and the duration of irradiations. The variation of fission product release as a function of these variables has been investigated extensively in the present study.

In addition to investigating the correlation between release and these factors, radiation effects such as dimensional change has also been analysed as volumetric change of the TRISO coated particle and is an important parameter in reactor design. The design of the defueling chute of the PBMR must take this into consideration as the diameter of the fuel pebble will have swollen as a result of radiation damage.

Based on the findings of the present research study the recommendations of how the research findings can be implemented to provide an improved PBMR fuel are made.

Dedication

In memory of my parents: Sentsó Populier Philip and Ntlemeng Johannah Leotlela.

Acknowledgements

I want to express my greatest gratitude to everyone who supported me throughout my postgraduate studies especially Tshepo Olifant my friend, my colleagues and most importantly the Management of PBMR Client Office for believing in me and their continued support, without whom this would not have materialised.

To Professor John Carter my mentor and my supervisor for his guidance and supervision throughout my postgraduate studies and for his persistent encouragement during the years of my in-service training at Schonland Research Centre for Nuclear Sciences (SRCNS), to Dr. Iyabo Usman for her continuous support and encouragement to never give up on the goals I have set myself, and to James Larkin for his valuable advice and guidance during the early days of research in fine-tuning my research proposal.

To Professor Piet Marais of Tshwane University of Technology who against all odds supported me in dark days of apartheid as a first Black Student in Nuclear Technology at Pretoria Technikon and gave me chance of a lifetime to realise my dream.

To Anthony Germishuys of the Computer Aided Learning Laboratory (Cal Lab) for his assistance with all analytical computer software (Mathtype, Matlab, Sigma Plot and Scientific word) I needed for my studies. To John Beer a “Friend of a Goodman” who walked with me every step of the way in the early years of my career in nuclear technology. Not only was he an excellent mentor, he was also excellent technical all-rounder who was able to switch from electronics to mechanical engineering without difficulty.

And last but by no means the least, to my family; Liz my lovely wife and our two adorable sons Kenneth and Thabo for their tireless support and being there for me whenever I needed them, above all for being the pillar of strength in my entire life.

Table of Contents

Declaration…….…….……..ii
Abstract……..…….……..iii
Dedication…….……iv
Acknowledgement…….……v
List of Figures……x
List of Tables……xii

CHAPTER 1: Introduction 1
1.1 Forecasting future energy demand for South Africa 1
1.2 Why Nuclear Energy?.....4
1.3 Rationale for selection of the Pebble Bed Modular Reactor (PBMR) technology.....5
1.3.1 PBMR short to medium-term objectives…….…...5
1.3.2 PBMR long-term objectives.....6

CHAPTER 2: Theoretical Background to the PBMR TRISO fuel 8
2.1 Basic technical characteristics of the Pebble Bed Modular Reactor..8
2.1.1 Temperature-Entropy Diagram…..……9
2.1.2 Reactor Pressure Vessel……...11
2.1.3 The 'Nuclear New Build' Project 13
2.1.4 Siting of Pebble Bed Modular Reactor 14
2.2 PBMR Fuel……14
2.2.1 Silicon Carbide.....17
2.2.2 Interaction of neutrons with materials.....23
2.2.3 Irradiation-induced crystalline-to-amorphous phase transition of SiC…….……..23
2.3 Precursors of silicon carbide failure 25
2.3.1 Interface reaction between silicon carbide and palladium …….25
2.3.1.1 Pd-SiC reaction mechanism 26

2.3.1.1.1 Investigation of corrosion by other researchers…….....30
2.3.2 Interaction of SiC with CO in TRISO fuel particles 32
2.3.2.1 Corrosion mechanism of SiC by carbon monoxide …….33
2.3.3 The role of internal gas pressure in fuel failure 34
2.3.4 Scenarios for determination of internal gas pressure 36
2.3.4.1 Pressure Vessel failure scenario 39
2.3.5 Yield of gaseous fission products and other associated gasses……..…..41
2.4 Modes of TRISO-coated particle failure 43
2.4.1 Category I failure mode 43
2.4.2 Category II failure mode 43
2.5 Diffusion of fission products through the TRISO coated particle layers…….....44
2.5.1 Vacancy diffusion mechanism 45
2.5.2 Interstitial diffusion mechanism.....46
2.6 Fission product release models.....47

CHAPTER 3: Experimental Investigation and Analysis 50
3.1 Description of the HFR Materials Testing Research Facility at Petten in The Netherlands.....50
3.1.1 Sample Holder……..……...50
3.1.1.1 Irradiation rig 51
3.1.2 Instrumentation 52
3.1.2.1 Process instrumentation 52
3.1.2.2 Nuclear instrumentation 54
3.1.3 Test samples and irradiation conditions.....55
3.2 Effects of irradiation of TRISO coated particle.....55
3.2.1 Fuel swelling and/or shrinkage 57
3.2.2 Effect of duration of irradiation on volume change 59

3.2.3 Correlation between change in neutron flux and volume change ……..61

3.2.3.1 Comparison with results of other investigations……. ……..63

3.2.3.1.1 Research conducted under the International Nuclear Energy Research Initiative (INERI).....64

3.2.3.1.2 Investigation by Argonne National Laboratory (US) and Bochvar Institute (Russia)…….……66

3.2.4 Correlation between increase in irradiation temperature and volume change…….……....68

3.2.5 Correlation between irradiation temperature and the diffusion coefficients of fission products 69

3.2.6 Gaseous fission product release phenomena.....70

3.2.6.1 Effect of variation of neutron flux with on fission product release……..71

3.2.6.2 Effect of changes in irradiation temperature on fission product release rate……...74

3.2.6.3 Effect of duration of irradiation on the release of fission product……..74

CHAPTER 4: Research Findings 79

4.1 Irradiation of TRISO coated particle results in crystal structure transformation of the SiC.....79

4.2 Long-lived fission products tend to dominate the release fractions .80

4.3 SiC is very susceptible to corrosion by metallic fission products and carbon monoxide 81

4.4 High Internal Pressure will lead to catastrophic failure of the SiC Pressure Vessel…….82

4.5 There is a link between the amounts of inert gas in the TRISO coated particle and the dimensional change it experiences.....82

CHAPTER 5: Conclusions and Recommendations.....84

5.1 Limiting operating conditions for the present fuel design.....84

5.1.1 Limitations imposed by the chemical composition of SiC ……84
5.1.2 Upper temperature limit 85
5.1.3 Aspects of PBMR Safety 85
5.1.4 Upper limit of the internal partial pressure. 86
5.2 Design fuels with better performance under irradiation conditions ..86
5.2.1 Formulate fuels that can form oxides with rare-earth fission products readily.....87
5.2.2 Add the second SiC layer between the buffer layer and the kernel ……87
5.2.3 Design a manufacturing process that will prevent formation of large grain boundaries 87
5.3 Include getter material in the fuel composition 88
5.3.1 Inclusion of an additional (SiC+PyC) layer as oxygen getter……88
5.3.2 Application of ZrC as an oxygen getter 88
5.4 Replace SiC with ZrC.....89

DEFINITIONS 91

ACRONYMS 93

REFERENCES.....95

List of Figures

Figure 1.1: Projection of future energy demand in South Africa……..…3

Figure 2.1: Power Conversion Unit of Pebble Bed Modular Reactor…….9

Figure 2.2: The PBMR T-S diagram……....10

Figure 2.3: The PBMR reactor pressure vessel [8, 10]…….....12

Figure 2.4: The TRISO Fuel element [8, 10]……...…….16

Figure 2.5: The schematic diagram of an HCP struture of SiC[25]……..…18

Figure 2.6: Schematic diagram of a BCC Structure of SiC…….....18

Figure 2.7: Schematic diagram of an FCC Structure of SiC……...…….18

Figure 2.8: The phase diagram of SiC, adapted from [29 and 34]……...21

Figure 2.9: Schematic representation of interaction of palladium with silicon carbide [38]……28

Figure 2.10: Schematic representation of corrosion by CO [41]……34

Figure 2.11: An illustrative diagram of a partial pressure of carbon monoxide as function of a ration of O/U [48]……35

Figure 2.12: Atomic oxygen released per fission of plutonium……39

Figure 2.13: A schematic illustration of vacancy diffusion mechanism [33]…46

Figure 2.14: A schematic illustration of the interstitial diffusion mechanism [33]……47

Figure 3.1: Fuel failure detection system [21]…….……51

Figure 3.2: Sample holder used at the HFR Material Testing Facility at Petten, The Netherlands [21]. …….…….…53

Figure 3.3: Core configuration illustrating sample irradiation position [21]…57

Figure 3.4: Coefficient of thermal expansion, α, of SiC……..58

Figure 3.5: Volume change of TRISO coated particle as function of irradiation time……60

Figure 3.6: Volume change as function of flux……62

Figure 3.7: The effect of fluence on the change in volume of TRISO coated particle……65

Figure 3.8: Swelling of β-SiC pyrocarbon as function neutron fluence [22]……65
Figure 3.9: Excess internal pressure as function of irradiation time [59]……67
Figure 3.10: Effect of irradiation temperature on % volume change……69
Figure 3.11: Diffusion coefficient of gaseous fission products…….70
Figure 3.12: Fission products release as function of neutron flux……76
Figure 3.13: Fission product release as function of irradiation temperature….77
Figure 3.14: Fission product release as function of duration of irradiation……78

List of Tables

Table 2.1: Redlich-Kwong gas constants[22, 49]……..……...37

Table **2.2**: Comparison of amount of free-oxyen released per fission of heavy metal as a function of Temperature ……...38

Table 2.3: Constants for the diffusion of gaseous fission products through the TRISO coated particle……49

Table 3.1: HFR K5 sample specification…….……56

CHAPTER 1

Introduction

As the population and economy of the country increase they exert a corresponding equivalent pressure on energy generation capacity to produce more energy to offset the demand and to sustain the growth. It is, therefore, critically important that an online feedback mechanism is built into the system that will incorporate these vital input parameters to indicate the amount of pressure they exert on the system and be able to make a projection of how much energy will be required to alleviate this pressure.

1.1 Forecasting future energy demand for South Africa

South Africa has experienced a considerable amount of economic growth in the past 10 to 15 years, thus demanding a corresponding growth in energy generation capacity. The mining industry is particularly known for consuming a significantly large proportion of the generating capacity because of their huge expanse compared to other industries, which subsequently puts a huge amount of strain on the present energy generation capacity. This is further exacerbated by the fact that quite a number of fossil fuel power stations have been mothballed i.e. the Power Stations were taken out of service for technical and/or economic reasons, adding more problems to the already strained generation capacity. Taking all these factors into account it is reasonable to expect that the demand for electricity will exceed the supply. This is particularly so when we take into consideration that there has not been any base-load power station built in that time frame. The load-shedding which was experienced in the first quarter of 2008 is testimony to the fact that the available generation capacity cannot cope with the demand; sending a strong signal that there is an urgent need for additional electricity generation capacity in South Africa.

Notwithstanding this, the Government of South Africa launched an Accelerated and Shared Growth Initiative for South Africa (AsgiSA) which aims at closing the gap between supply and demand, and has made a projection that South Africa will need as a minimum an increase in its present capacity by 40 000 MW in the next twenty years [1]. In order to meet that target, the nuclear energy policy of South Africa was developed which delineates generation responsibilities between the Government and Independent Power Producers (IPP). It is envisaged that the Government will be responsible for 70% of the new power generating capacity, while IPPs will supply the remaining 30% [2].

In the recent Environmental Impact Assessment (EIA) conducted by Arcus Gibb [3] it was established how that demand for electricity in South Africa varies from region to region and also with the time of the day. The shortage in various regions was compounded by the fact that a large amount of energy generation capacity is based inland, resulting in energy distribution via long transmission lines to areas where it is needed. The energy loss due to the impedance of the transmission lines adds to the shortage. Given that 90% of the coal resources from which South Africa generates its electricity are located in the eastern part of the country and the demand for electricity is throughout the country, with the mining and industrial sectors accounting for approximately 40% of the electricity demand, puts a further strain in the generation capacity [3].

It will be appreciated that the presently installed electricity generation capacity is only about 40 000 MW, inclusive of all power generation, leaving a reserve margin of 5-10% for emergency supply; far less than the internationally recommended norm of 15% to avoid load-shedding. In this context, load-shedding is a controlled way of rotating the available electricity between all customers, thus ensuring that the impact of electricity shortage is spread around the country or provinces and not just confined to a single area. The projection of future energy demand is illustrated in Fig. 1.1.

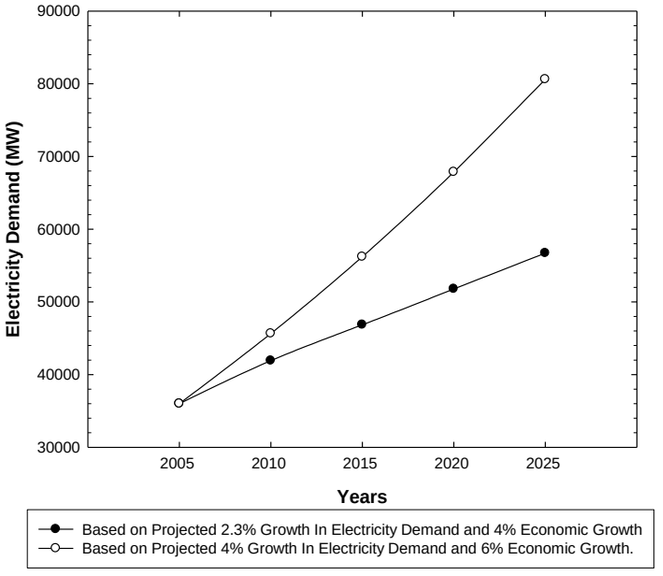

Figure 1.1: Projection of future energy demand in South Africa (present study).

A further energy demand forecast [3] based on population and economic growth indicates that the increase in energy generation capacity will have to be drastically accelerated to avoid the 2007 load-shedding experience from being the norm. Taking these factors into consideration, there is little doubt that the projected future energy needs of South Africa in 2025 is expected to increase by between 40 000 MW and 60 000 MW in addition to the present generation capacity, depending on the projected percentage in economic and population growth.

Figure 1.1 provides a graphical representation of this projection. The bottom line represents the energy projection based on a conservative 4% economic growth rate while the top line makes allowance for the AsgiSA economic growth rate target of 6% [1]. It is clear from this figure that at a 6% economic growth rate, the Government will have to make accommodation for approximately 80 000 MW (40 000 MW additional to existing capacity) by the year 2025 while at the conservative economic growth rate of 4% the Government will need to

make allowance for approximately 60 000 MW (20 000 MW additional to existing capacity).

1.2 Why Nuclear Energy?

In terms of the South African legislation, the Government is required to include as many energy generation options as possible in its energy mix. One such regulation which has to be taken into consideration is regulation R. 385 in terms of National Environmental Management Act (NEMA) which makes this mandatory [4]. However, in spite of this, there are certain limitations in using other options to generate electricity. For example, it is a known fact that coal is notorious for emitting noxious gasses which have a negative effect on climate change and on the environment. In terms of the Kyoto Protocol, South Africa is bound by the conditions of the protocol to either reduce its present CO_2 emission or at least keep it at its present level [5], which rules increased use of fossil fuel out of the energy mix. Other options such as gas, wind, solar and hydroelectric power have intermittent generation capacities, making them very unreliable and, therefore, unsuitable for base load supply. This leaves the Government with little choice but nuclear.

Although, technically, nuclear energy is the most preferred form over all others because of its low impact on climate change, socially it is a different story; there is still tremendous resistance against nuclear energy in spite of all the efforts being done to change public perception. The recent court case in the Cape High Court in which Earthlife Africa successfully appealed against the Positive Record of Decision (RoD) issued by the Director General of the Department of Environmental Affairs and Tourism was set aside is a classical example illustrating the challenges facing nuclear energy compared to other forms and the fact that globally nuclear power is still not acceptable [6].

1.3 Rationale for selection of the Pebble Bed Modular Reactor (PBMR) technology

Because of the urgency to bridge the gap between energy supply and demand, the Government has identified a number of projects aimed at preventing the situation from getting worse and at the same time meeting future energy demands. This includes, among others, refurbishing all those power stations which were mothballed and bringing them back into operation. However, the selection of new projects was based on a number of important techno-economic factors which include efficiency, safety features and reliability of the technology. Taking all these criteria into account, the Pebble Bed Modular Reactor (PBMR) came up at the top. In order to resolve its energy generation problem, the Government divided its efforts into short to medium term and long term objectives, each with a specific milestone in the entire project.

1.3.1 PBMR short to medium-term objectives

In the short to medium-term, a safe, reliable and efficient reactor technology is required to demonstrate the technical and economic viability of the technology that is comparable to other technologies available on the market. The economic viability was based on the cost of generating energy (cost per kW), i.e. the cost of generating electricity by a selected technology must be comparable to the cost of generating with other equivalent comparable technologies on the market i.e. generation from nuclear must not be more expensive than generation from fossil fuel or solar energy, and among the nuclear options, High Temperature Gas Cooled Reactors (HTGR) must be comparable to Light Water Reactors (LWR) or Boiling Water Reactors (BWR). This resulted in the PBMR emerging as the most favourable technology. Indeed, the Government is in a process of licensing a 400 MW(th) Pebble Bed Modular Reactor Demonstration Power Plant (PBMR DPP) designed by PBMR (Pty) Ltd, a state owned entity accountable to the Ministry of Public Enterprises, to be located at the Koeberg Nuclear Power Station (KNPS) site in the Western Cape Province [3].

1.3.2 PBMR long-term objectives

The long-term objectives of the PBMR include the following:

1. Modular design enabling more efficient and cost-effective expansion of the electricity generation capacity at a single location. Because of the modular nature of this design, more reactor modules can be added to the existing unit without spending an exorbitant amount of money because resources that are common to all are shared between reactor modules. In that way the cost of generating electricity is reduced.
2. The PBMR design is aimed at achieving a plant with a radiation hazard well below what is currently acceptable for Light Water Reactors. This would prevent the social impacts associated with large emergency planning zones (EPZ) and the corresponding restrictions on development within these zones [7].
3. Significantly reduced amount of high-level radioactive waste.
4. The cost per unit of electricity generated must be comparable to other low cost electricity generation options such as fossil fuel power stations.
5. The PBMR design is envisaged to have a combination of active and passive safety systems in order to ensure that the plant operates safely at all times, and if it were to operate in an abnormal condition, no member of the public would be exposed to undue radiation exposure, which is consistent with the As Low As Reasonably Achievable (ALARA) principle [4].
6. Proliferation resistant: the PBMR does not produce as much plutonium as other types of reactors do and since the spent fuel is kept on site until the end of its life, the security risk of being tampered with is reduced.
7. High efficiency: the PBMR has a much better efficiency (43%) compared to Light Water Reactors which have an efficiency of 33%. In financial terms this translates to more kWs power for PBMR generated per unit cost than is the case with Light Water Reactors [8].
8. Reduced reliance on fossil fuels as the primary energy source for generating electricity, thus making a significant reduction on carbon emission.

9. Multi-purpose use of the technology: investigations done to-date suggest that the PBMR technology could also be used effectively in the process heat industry. Two potential clients of importance to PBMR (Pty) Ltd in South Africa that could benefit tremendously from the process heat application of PBMR are Sasol and Caltex. This is because some of their chemical processes e.g. the gasification and hydroxylation processes at Sasol are endothermic, requiring an input of energy to initiate or sustain their chemical reactions. These are processes that can benefit hugely from an excessive amount heat energy liberated from PBMR nuclear processes which significantly reduce their reliance on Eskom for energy supply.

10. In addition to process heat and power generation application, PBMR can be applied to desalination of sea water. This is particularly suitable to West African countries which have been classified as water-stressed but have access to sea/ocean water. To-date the focus of marketing PBMR has always been on power generation and process heat application, not enough effort has been made to market this technology in water desalination application.

The structure of this Research Report is as follows:

- **Chapter 2, Theoretical Background to the PBMR TRISO fuel:** this chapter provides a theoretical basis of fuel qualification of TRISO-coated particle based on literature survey with the view of indicating what research has been done in this area to understand fuel failure and fission product migration mechanisms.
- **Chapter 3, Experimental Investigation and analysis:** this chapter provides the description of instruments and the experimental layout that was used in the detection of fission products.
- **Chapter 4, Research findings:** in this chapter, the Research Report provides a detailed account of the findings which were obtained in this investigation.
- **Chapter 5, Recommendations:** the focus of this chapter is to summarise recommendations, based on the findings discussed in Chapter 4 that will have to be implemented to minimise deterioration of fuel quality and subsequent fission product release.

CHAPTER 2

Theoretical Background to the PBMR TRISO fuel

After Roy Huddle invented the coated particle in 1957 in Harwell, 15 years later he remarked "*Now that we know everything about coated particles, we should be going on to deal with other problems*" [68]. Little did he know that the problems with fuel design are only a tip of the iceberg. Real problems were only beginning to emerge when the fuel is being irradiated, with fission product release being symptoms of much greater and deeper underlying problems which we are only now beginning to understand. The real solution to these problems lies in the knowledge and understanding of every aspect of what leads to fuel failure. These among others include: understanding the reaction mechanism between neutrons and the isotopes out of which the fuel is made, crystal structure transformation resulting from the interaction between the fuel and neutrons, fuel failure mechanisms and the migration mechanism fission products utilise to migrate through various layers of the TRISO coated particle-regardless of whether it is diffusion or otherwise.

2.1 Basic technical characteristics of the Pebble Bed Modular Reactor

The PBMR consists of a graphite-moderated, helium-cooled reactor in which the gas is heated by the nuclear fission process, and a direct-cycle power conversion unit in which the heat is converted into electrical energy by means of a turbine-driven generator. The reactor core is based on High Temperature Gas Reactor (HTGR) technology, originally developed in Germany [8, 9]. PBMR uses spherical fuel elements, called pebbles that are identical in size and physical characteristics as the fuel first developed for the German AVR reactor, where AVR is an acronym for Arbeitsgemeinschaft Versuchs Reaktor [8, 9].

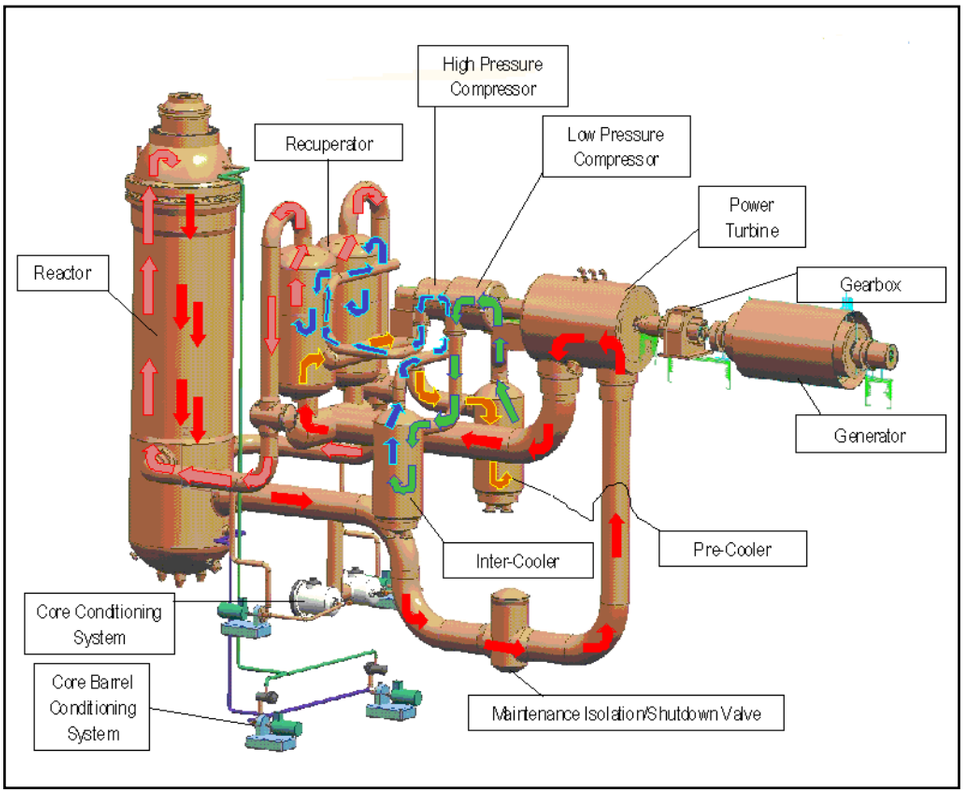

Figure 2.1: Power Conversion Unit of Pebble Bed Modular Reactor.

Instead of using the German power conversion configuration (gas-to-steam cycle heat exchanger), the PBMR utilises a direct cycle power conversion configuration [8, 10, 11]. The design layout of the PBMR is shown in Fig. 2.1.

2.1.1 Temperature-Entropy Diagram.

In order to understand the PBMR concept, it is necessary to follow the Temperature-Entropy (T-S) diagram illustrated in Fig. 2.2 and at the same time follow the process flow diagram indicated by the arrows in the Power Conversion Unit (PCU) illustrated in Fig. 2.1. In addition, Fig. 2.1 provides the component layout of the system while Fig. 2.2 will help to understand the process. Beginning at Stage 4 of Fig. 2.2, the low pressure and temperature helium is compressed by a Low-Pressure Compressor (LPC), to an intermediate pressure at Stage 5 [10]. The gas is then cooled in an intercooler to Stage 6.

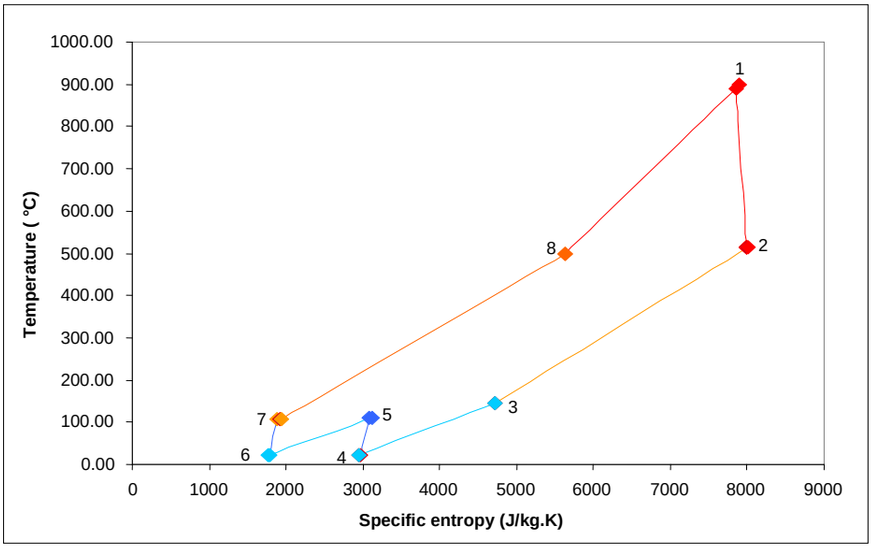

Figure 2.2: The PBMR T-S diagram.

The intercooling (Stages 5 and 6) between the two compressors improves the overall cycle efficiency. The High-Pressure Compressor (HPC) compresses the helium (Stage 7), and between Stages 7 and 8, the helium is preheated in the Recuperator before entering the Reactor where it is heated (Stage 1).

As the gas exits the reactor it is expanded into the Power Turbine which drives the LPC and HPC. The excess power is used to drive the Generator via a gearbox. Between Stages 2 and 3, the hot helium is cooled in the recuperator, after which it is further cooled in a Pre-cooler to Stage 4. The recuperator uses heat from the cooling process that would otherwise be lost to the main heat sink. This heat is used to increase the temperature of the gas before it enters the reactor, thereby reducing the heating demand on the reactor and subsequently increasing the overall plant efficiency. For the purpose of safety, the operating temperatures are set below 1200°C with the limit being set at 1130°C. This is done specifically to prevent any fission products from escaping through the barriers of the TRISO coated particle since diffusion is a function of temperature.

2.1.2 Reactor pressure vessel

The primary purpose of the Reactor Pressure Vessel (RPV) which is indicated in Fig. 2.3 [8, 10] is to provide the entire plant with the reactor vessel of correct geometry where fission reactions can take place under controlled conditions [12, 13]. It consists of the reactor unit, the core barrel assembly, the core structure ceramics and the reactivity control systems by means of which the criticality of the reactor is controlled. To prevent criticality going out of control the reactor has 24 control rods distributed evenly throughout the reactor core where the reaction takes place. The temperature of the RPV is maintained by a continuous flow of helium gas that flows though the reactor at rate of 13.6 kg s^{-1} at the pressure of 9.0 MPa. It is designed to protect the fuel from reaching high temperatures by allowing for the high availability of active cooling, thus keeping the fuel temperature from rising beyond the design limit.

The RPV is made up of a number of internal components (see Fig. 2.3) which collectively provide the reactor vessel with sufficient volume and the correct geometry in which nuclear reactions can take place with minimal risk of Reactivity Induced Accidents (RIA). One of the main functions of the internal components of the RPV is to reduce the probability of severe nuclear accident from taking place.

This is achieved by:

- Providing and maintaining the correct geometry at all times regardless of the operating mode of the reactor. This is an important design consideration which distinguishes PBMR technology from PWR and BWR reactor designs since these lose their core geometry under extremely high temperature conditions and result in core melt accidents.
- Provide and maintain flow path of fuel spheres.
- Provide and maintain openings for the reactivity control and shut down systems. This is the most important safety consideration in reactor physics since the operator must at all times be able to control neutron multiplication in the reactor, and the control systems are the only means by which the

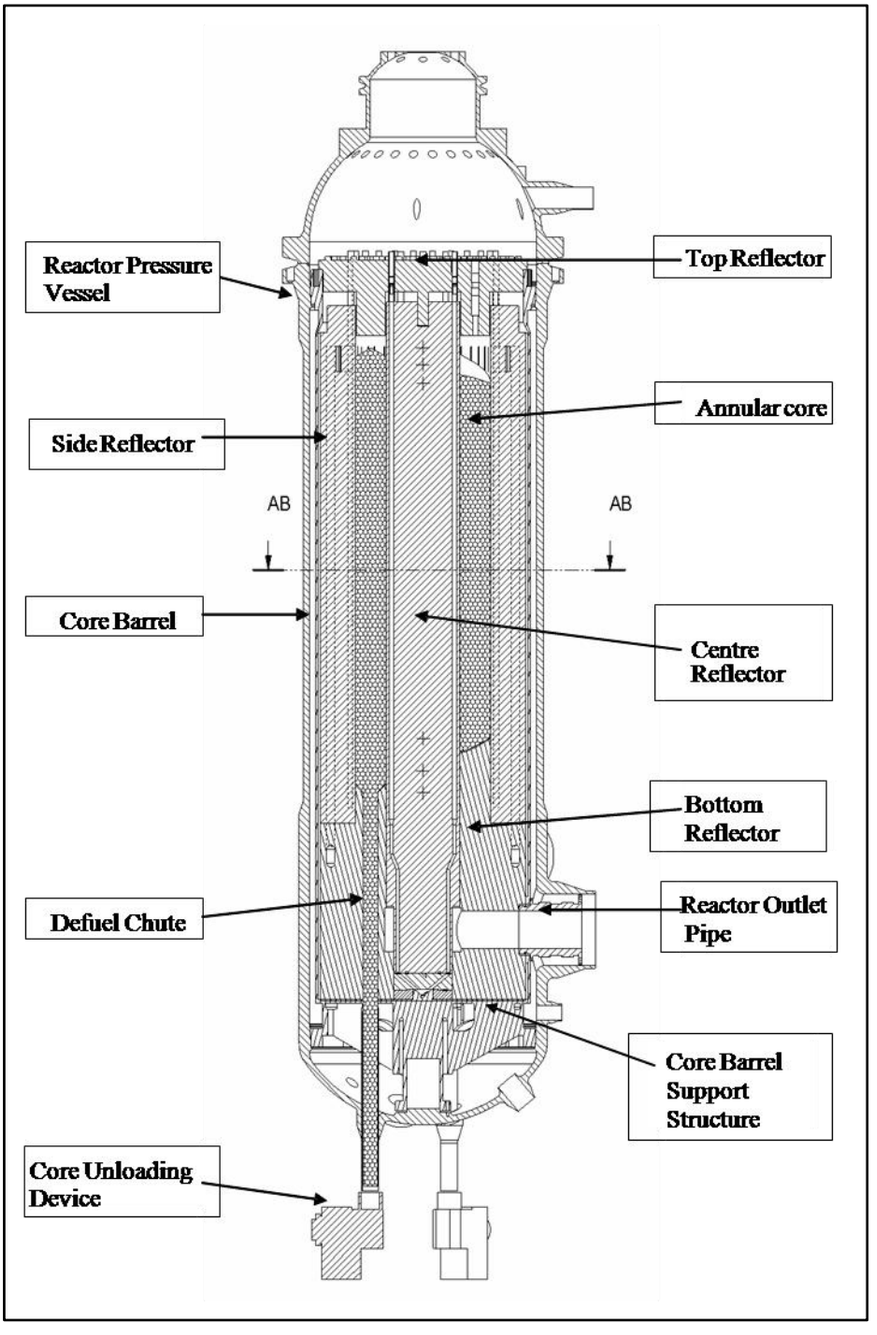

Figure 2.3: The PBMR reactor pressure vessel [8, 10].

operator can manually control neutron multiplication and hence the reactivity of the reactor.

- Acting as neutron reflectors, to reduce the neutron energy as well as providing the necessary shielding against neutrons and gamma rays.

These are particularly important considerations in reactor safety design since reactivity induced accidents are directly related to criticality of the reaction which among others can be caused by air and/or water ingress in the vessel.

2.1.3 The 'Nuclear New Build' Project

In addition to the PBMR project, the Government has, under the auspices of Eskom, initiated a second nuclear project intended to complement the present energy generation capacity. No firm decision has yet been made as to the type of reactor to be built. This project has recently been put on hold as a result of the global economic crisis, however, other sub-projects which had already been initiated to obtain the nuclear licence are continuing. These include amongst others conducting the Environmental Impact Assessment (EIA) of three potential nuclear sites *viz*. Duynefontein, Bantamsklip and Thyspunt and was scheduled to go for public comment in May 2009 [14]. The compilation of the Site Safety Report (SSR) of the Thyspunt nuclear site is at an advanced stage and could be ready for submission to the National Nuclear Regulator (NNR) early in 2010. The Site Safety Report in this context refers to the report required by the National Nuclear Regulator in terms on the Nuclear Energy Act that contains the results of the analysis to determine whether it meets all the safety requirements to build and operate the nuclear plant [4, 15, 16].

The siting of the PBMR is subjected to equally stringent siting regulations since its design is based on internationally accepted norms and international best practices. Thus, if the site is deemed acceptable by the National Nuclear Regulator, it will be found equally acceptable by any other independent Nuclear Regulatory Authority evaluating the suitability of the site. To that effect the most

suitable site for PBMR has been found to be the Koeberg nuclear site for reasons discussed below.

2.1.4 Siting of Pebble Bed Modular Reactor

With regard to siting of the PBMR, a number of alternative sites were investigated in line with the requirements of the Environmental Conservation Act of 1989 and the Environmental Impact Assessment Regulation published in Government Notice no. R 1183 [3]. However, based on safety considerations recommended by the International Atomic Energy Agency (IAEA) in siting of nuclear installations, none of them were found suitable except for the Koeberg nuclear site. This benefitted the PBMR project tremendously since the site is already licensed and PBMR could also benefit from infrastructure resources it would share with Koeberg [17]. Even the Government stands to benefit a great deal from siting PBMR at Koeberg since this is the only Power Station in the Western Cape, as a result a significant amount of energy is lost in the transmission process from power stations situated in Provinces that are inland. In addition, the PBMR will play a significant role in alleviating the pressure of demand on the National Electricity Grid, especially in the Winter seasons, as well as help stabilise the Western Cape electricity grid by complementing Koeberg's generation capacity in that province [18, 19].

2.2 PBMR fuel

The PBMR fuel sphere, generally known to as the pebble, is a 60 mm spherical pebble made up of ~ 15 000 Tri-Isotropic (TRISO) coated particles that are 0.92 mm in diameter, distributed evenly within the fuel sphere and surrounded by the graphite moderator. A single pebble contains 9 g of uranium in the form of UO_2 enriched to 9.6% with ^{235}U, which is an important fissile material for the fission process. Generally a PWR such as Koeberg has an average enrichment of 4.5%, an average fuel cycle[1] of 3 cycles and ZrC as a fuel cladding. One cycle in this

[1] One cycle is time the fuel spends in the core before the next refuelling outage.

context refers to a fuel burnup (BU) of 20 000 MWd/tU (~365 days), depending on the BU the cycle can be extended to a maximum of 62 000 MWd/tU (~ 547 days) and at the end of each fuel cycle the fuel assembly is repositioned towards the centre of the core for the next cycle. Although PBMR fuel has twice as much enrichment as PWR fuels do and from this one is tempted to believe that this justifies a longer effective full power days in the core, the fact that the cladding of Koeberg is ZrC which is much more resistant to irradiation than PBMR's SiC and that the exposure of Koeberg fuel to neutron flux is gradually increased; starting on the outside of the core and moving one step each cycle to the centre of the core, taking a total of 3 cycles get to the centre, and since PBMR fuel on the other hand does not have this gradual approach to the centre of the core, this off-sets the higher enrichment advantage PBMR fuel has over Koeberg's fuel. The gradual approach to the centre of the PWR fuel makes the actual period spent in the centre of the core much less than the maximum 547 days allocated for the fuel run, which makes 923 days to be too long to irradiate the TRISO fuel [10, 80]. The TRISO coated particle plays a significant role in the safety of the PBMR-it is the primary containment of fission product migration. A schematic diagram of the TRISO fuel is shown in Fig. 2.4 indicating that in addition to acting as a containment for fission product migration, it also acts as a pressure vessel in which the fission reactions take place [20]. As shown in Fig. 2.4, the TRISO coated fuel particle is made up of several layers, each of which plays a distinctive role in the reliability and effectiveness of the fuel in retaining fission products within the barriers of the TRISO coated particle.

The fuel particle comprises the following:

- **Kernel:** This is the actual UO_2 sphere that is enriched to 9.6% with ^{235}U and is 500 μm in diameter. Its primary function is to provide the ^{235}U fissile material in the correct atom density to enable fission reaction to take place at the rate that is just sufficient for the process to be critical and sustain itself. Additionally, it also constitutes the first barrier of release of fission products.

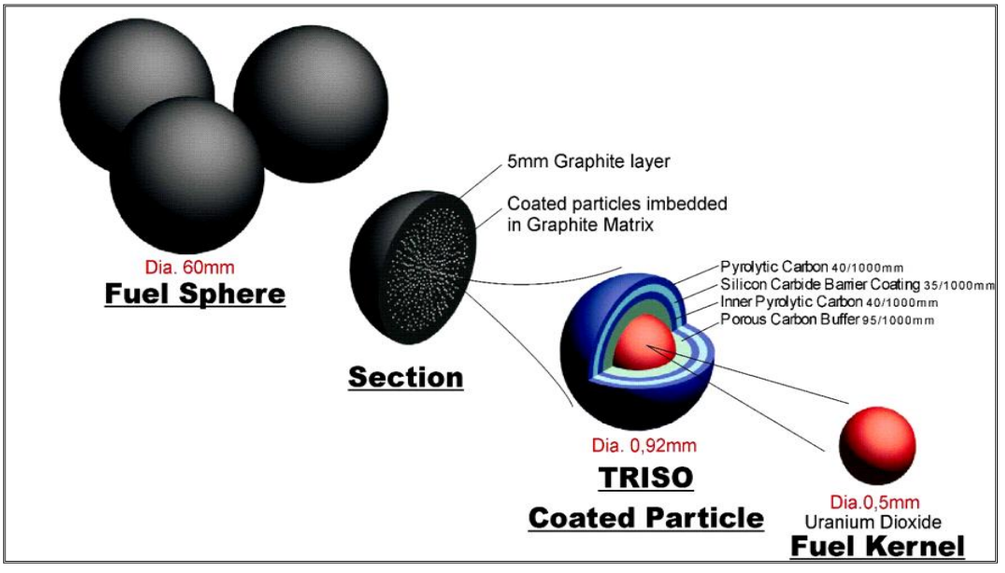

Figure 2.4: The TRISO Fuel element [8, 10].

- **Buffer:** The buffer layer is a porous pyrocarbon layer which is 95 μm thick. Its primary function is to provide room to accommodate for the expansion of gas from the fission process as well as the swelling of the fuel kernels during irradiation. It also protects the inner PyC from radiation damage due to recoil of fission fragments from the kernel.

- **Inner Pyrolytic Carbon (IPyC):** The IPyC layer is 40 μm thick and has the function of preventing the reaction between the kernel and chlorine gases released during the decomposition of SiC. Chlorine gas was introduced in the fuel during the manufacturing process. The IPyC constitutes the second barrier against fission product release.

- **Silicon Carbide (SiC):** The SiC is 35 μm thick and is the main load-bearing component of the SiC and the main barrier against fission product release.

- **Outer Pyrolytic Carbon (OPyC):** The 40 μm thick OPyC serves to protect the SiC layer from mechanical damage during the fuel manufacturing process and provides an additional barrier against fission product release.

Based on this, it is therefore imperative that whenever reactor safety and accident analyses are conducted, the role of SiC as a confinement of fission product is also taken into consideration. The ability of the SiC to withstand high tensile stress from internal gas pressure generated during fission process is of prime importance in reactor safety analysis and also to public safety [21]. From the reactor safety point of view, the most important aspect of the SiC layer is its high Ultimate Tensile Strength. That explains why it is such an important parameter in estimating fuel failure probability [22]. The safety of PBMR relies heavily on the ability of this layer to prevent the escape of fission products from the fuel kernel. From this, one can infer that the outer three layers (IPyC, SiC, and OPyC) all together act as a pressure vessel for gaseous fission products as well as barriers to the migration of other fission products [20].

2.2.1 Silicon Carbide

Silicon carbide is one of the most important materials in technology generally because of its semiconducting properties, high temperature stability, extreme hardness and chemical inertness. In nuclear technology, it is of particular interest because of its low neutron-capture cross-section. Structurally, it is a polymorphic material capable of existing in more than 100 crystal structures, which are classified as either alpha-SiC (α-SiC) or beta-SiC (β-SiC):

- The α-SiC is depicted by Fig. 2.5. It is also known as the (6H-polytype) or simply the hexagonal close-packed (HCP) unit cell. The form shown in Fig. 2.5 is further divided into a number of variations within itself which among others includes 2H-SiC, 4H-SiC and 6H-SiC [23, 24, 26, 27, 28].
- The β-SiC or more commonly known as the 3C-polytype is the cubic polytype of the SiC and it too is divided into a number of subcategories according to spatial arrangement of atoms in relation to one another. These, among others, include the Body-Centred Cubic (BCC) depicted in Fig. 2.6 and the Face-Centred Cubic (FCC) depicted in Fig. 2.7.

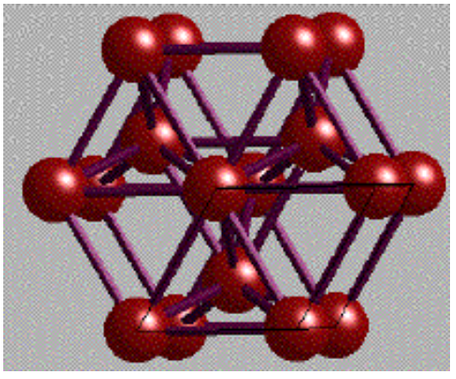

Figure 2.5: Schematic diagram of an HCP structure of SiC [25].

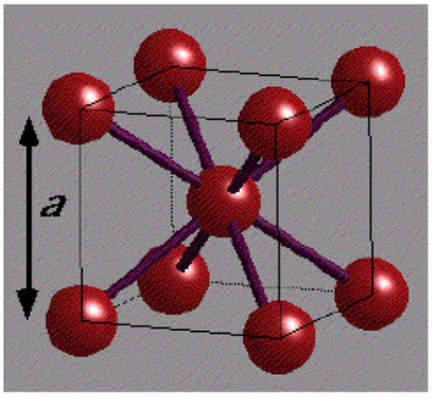

Figure 2.6: Schematic diagram of a BCC structure of SiC [25].

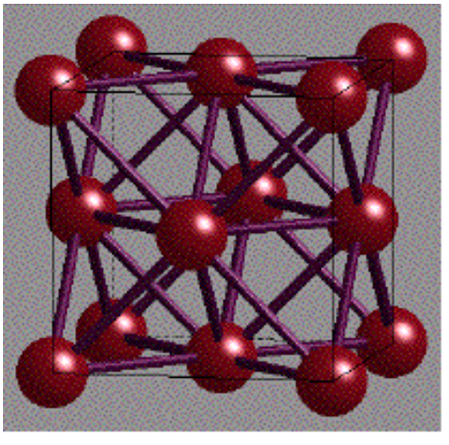

Figure 2.7: Schematic diagram of an FCC structure of SiC [25].

Other polytypes that are often encountered in material science include the 15R-SiC (rhombohedral unit cell), with variations 21R-SiC, 24R-SiC and 27R-SiC [23, 24, 29]. Material physics knowledge of TRISO coated particles is significantly important to fuel scientists and to safety engineers since it provides them with a basis of how the material may react under varying temperature and radiation conditions. From this, Monte Carlo techniques can be used to determine the probability of failure and their subsequent radiological consequences. It has been established that although there are several polytypes of SiC, they are inter-convertible from one crystal structure to another [30]. For example, in 1996 Weber [26, 31, 32] discovered that under high temperature and harsh irradiation conditions SiC undergoes amorphisation changing from one crystal structure to another.

This was further confirmed by Rugirello *et al.* and Weber [26, 28, 33], who established that there is a temperature limit below which crystal structure transformation can continue unhindered, beyond that temperature, amorphisation cannot take place. Also, in 2007 Krishna [29] was able to show that 2H-SiC (α-SiC) was easily transformed to 3C-SiC (β-SiC) in an argon atmosphere at 1400°C, which is a further confirmation to the temperature dependence of amorphisation referred to earlier and is confirmed by the phase diagram of SiC depicted in Fig. 2.8.

In a nuclear reactor core where there is a combination of both high temperature (900°C) and high neutron flux ~ $1x10^{15}$ n cm^{-2} s^{-1}, amorphisation begins to take place even earlier than the suggested temperature range. In addition to temperature dependence, it has been shown that other factors such as the presence of impurities greatly enhance amorphisation, which provides an explanation why under high neutron flux and high temperature conditions the amorphisation process can be initiated much earlier. It has been reported that when transformation takes place it occurs in phases, depending on what the state of matter that material is in at that time, and the duration of the transformation may either be short or longer depending on the neutron flux, irradiation time,

irradiation temperature, and the free-energy of the crystal structure at its destination [33].

Looking at Fig. 2.8 and drawing a straight line vertically upwards from 30% carbon concentration through F, it is observed that the material below the solidus line defined by 1415°C, is a solid made up of α-SiC and SiC in equilibrium with each other. The temperature will stay constant at 1415°C until all the α-SiC has melted. Above this temperature, all the α-SiC has melted and SiC is still in a process of melting, and will remain in the molten phase until it has reached 2830°C where all the SiC has completely melted and only carbon from α-SiC is left in equilibrium with liquid.

Although it is highly unlikely that the operating temperature will ever reach 3000°C without an intervention, it is worth noting that when the temperature reaches the liquidus line at 3000°C, the material above the liquidus line and on the left of the 30% line is completely liquid while the material right of the 30% line is a liquid phase in equilibrium with carbon.

As the temperature continues to increase it reaches the point (~3525°C) where the TRISO coated particle has completely melted. If a tie-line AB is drawn at this temperature, i.e. (~3525°C) such that point A coincides with the vapour-line and point B with the liquid line, by using the lever-rule, the 30% concentration line will divide the tie-line into two parts whose lengths are inversely proportional to the amount of the phase present [23, 24].

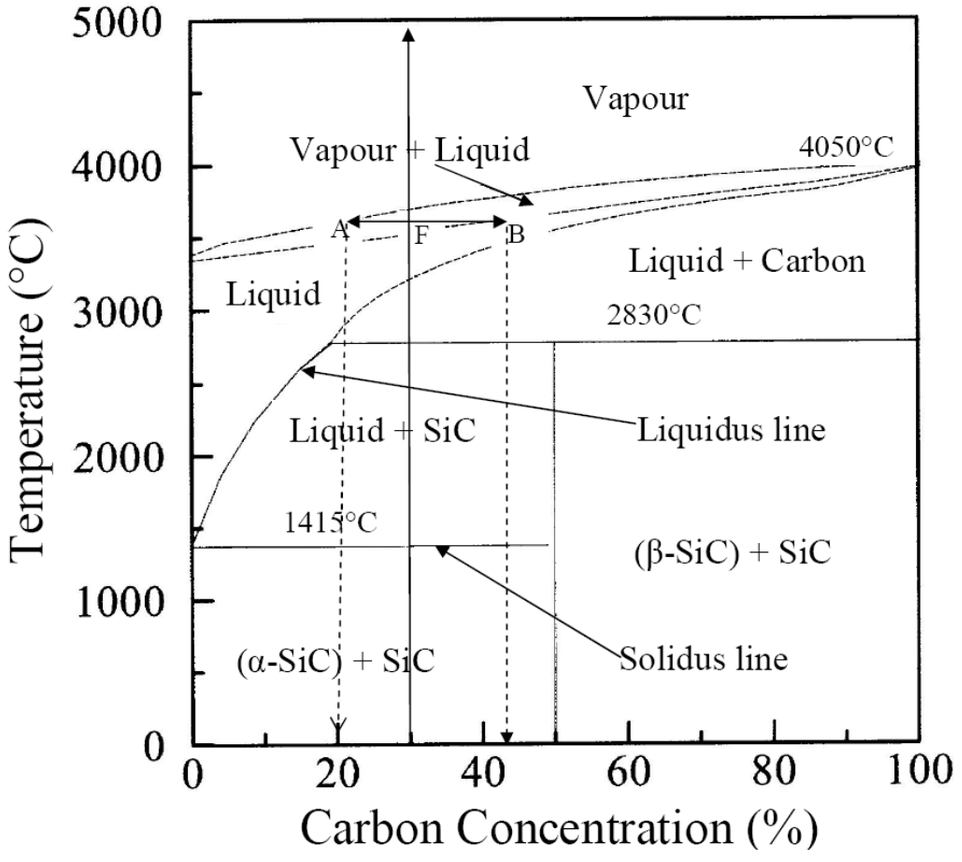

Figure 2.8: The Phase diagram of SiC, adapted from [29 and 34].

The point where 30% vertical line intersects the tie-line is considered as the fulcrum, F, of the lever system. If the entire length of the tie-line AB is taken to represent 100% of the total weight of the two phases present at temperature T ~ 3525°C, the fraction of the material in each phase may be determined by means of the Lever Rule which may be expressed mathematically as

$$V_{\mathrm{p}} = \frac{FB}{AB} \times 100\%, \tag{2.1}$$

where V_{p} refers to the vapour phase. This indicates the total amount of material that will be in the vapour phase. The concentration at points A and B is found by drawing a vertical line from A and B respectively to the carbon concentration line and the concentration at these points is read at the point where the two vertical lines meet the carbon concentration line. Thus, the concentration at points A and B are found to be 20% and 41.25%, respectively. Therefore, the lengths of FB and AB are found to be:

- FB = 41.25% − 30.00% = 11.25%
- AB = 41.25% − 20.00% = 21.25%.

Hence, if FB and AB in Eq. (2.1) are replaced by 11.25% and 21.25% respectively, this results in V_{p} being:

$$V_{\mathrm{p}} = \frac{11.25}{21.25} \times 100\%, \tag{2.2}$$

which leads to 52.94% of the material being in the vapour phase, and the amount of the material in the liquid phase, L_{p} is obtained from:

$$L_{\mathrm{p}} = \frac{AF}{AB} \times 100\%, \tag{2.3}$$

where L_{p} refers to the liquid phase. Considering that AF and AB are 10% and 21.25%, respectively, it implies that

$$L_{\mathrm{p}} = \frac{10}{21.25} \times 100\%, \tag{2.4}$$

which results in 47.06% of the material being α-SiC.

This provides additional confirmation that at no stage should the TRISO coated particle be subjected to temperatures higher than 1415°C, let alone any temperature degree beyond that. The β-SiC follows the same description except it does not pass through the liquid+SiC phase, at 2830°C it is all liquid in equilibrium with carbon.

2.2.2 Interaction of neutrons with materials

When neutrons interact with matter they create Primary Knock Atoms (PKA) and the damage resulting from the transfer of energy from an incident projectile to the target material subsequently results in the creation of a collection of point defects (vacancies and interstitials) and clusters in a crystal lattice [30, 33]. Bombardment of SiC with neutrons results in the neutron interacting with either the silicon or the carbon. In either case, this may either be an elastic or an inelastic scattering reaction. Which one of these nuclides is hit first depends on a number of factors, the most important being the atom density of the target (SiC), the other being the interaction cross-section of the two nuclides, silicon and carbon [13, 35, 36]. The amorphisation fraction, f_a, is given by [31]

$$f_a = 1 - \left(\sigma_a + \sigma_s \right) \Big/ \left(\sigma_s + \sigma_a \exp\left[\left(\sigma_a + \sigma_s \right) D \right] \right), \tag{2.5}$$

where σ_a is the amorphisation cross-section, σ_s the effective cross-section for defect stimulated amorphisation and D is the neutron dose. This is a very valuable relationship since it indicates the temperature independent link between the probability of a reaction (cross-section), the neutron dose (D) and the fraction of materials that has undergone transformation.

2.2.3 Irradiation-induced crystalline-to-amorphous phase transition of SiC

Amorphisation of SiC has attracted a lot of interest in nuclear technology because of potential opportunities that SiC can offer as a cladding material for nuclear

fuel. However, there are disadvantages. This is particularly the case for SiC-clad TRISO fuel particles because as the material changes from α-SiC to β-SiC there is a corresponding increase in fission product release, which suggests that as SiC undergoes transformation, its ability to retain fission products is impaired. Because of the high temperature and high neutron dose in which the SiC is exposed during the operating life of the reactor, it has been found that amorphisation takes place very readily in SiC, with the critical temperature (T_c) varying from 21.85°C to 211.85°C for α-SiC. During the investigation of the effect of temperature on amorphisation, Weber [26] found that amorphisation increases more rapidly as the fuel temperature increases, and also with the increase in the energy of projectile. The general relationship between temperature and dose required for complete amorphisation is given by [32]:

$$\ln\left[1- D_0/D^{m}\right] = C - E_a / nkT, \tag{2.6}$$

where

D_0 = dose for complete amorphisation at −273.15°C

E_a = activation energy (~ 0.1 eV)

C = constant dependent on ion flux and damage cross section, and m and n are the model dependent constants, and may take the values m = 1/2, 1/3 or 1 and n = 1 or 2

D = the dose or flux.

The cut-off temperature T_c is defined as

$$T_c = E_a/kC, \tag{2.7}$$

where k is Boltzmann's constant.

The above two equations demonstrate two most important aspects of radiation damage of SiC that are critical to fission product release, namely,

- There is temperature limit for SiC above which amorphisation does not occur regardless of the dose and type of projectile, but below that temperature there is a causal relationship between temperature and amorphisation.

- There is direct link between the fraction of SiC that undergoes amorphisation and dose received.

Hence, the temperature and dose to which the TRISO fuel is exposed in the reactor will have to be monitored carefully in order not to exceed the limit that will eventually lead to high fission-product release. The detail of how the temperature and flux relate to release rate is described in detail in Chapter 3 of this Research Report.

2.3 Precursors of silicon carbide failure

Fission product release is preceded by a number of factors that lead to SiC failure before the release actually occurs and eventual failure of the entire fuel sphere. These include, amongst others, an increase in partial pressure resulting from an increase in the amount of gaseous fission products and their kinetic energy as a resulting of an increase in fuel temperature, which subsequently result in an increase in tensile stress on the SiC. This is further compounded by the fact that metallic chemical reaction with SiC weakens the SiC which eventually leads to its failure.

2.3.1 Interface reaction between silicon carbide and palladium

Palladium is one of the fission products generated during the fission process in UO_2 fuel [37]. Although there are other metallic fission products such as Cr, Zr and Ni that are produced, Pd is of greater importance in SiC-clad fuel because of the detrimental effects of its chemical reaction with the SiC [38]. The interaction between SiC and metals has been investigated extensively in nuclear technology with a view to understanding the cause of degradation of SiC's ability to retain fission products within the particle, which is regarded as one of the main factors leading to SiC failure and eventually results in the release of fission products. The possibility of interface reaction between the matrix and the reinforcing material

may lead to structural instability and thereby deterioration in mechanical properties of the composite [39].

2.3.1.1 Pd-SiC reaction mechanism

During the study of palladium interaction with silicon carbide Minalto *et al*. [39, 40] reported that the corrosion morphology of SiC was primarily due to the following reaction:

$$2Pd + SiC \rightarrow Pd_2Si + C. \quad (2.8)$$

The Pd accumulates at the IPyC-SiC interfaces and reacts with SiC according to Eq. (2.8). It has been shown that the corrosion was dependent on temperature gradient, with greater accumulation of Pd on the colder side of the coated particle than on the hotter side [41]. In addition to establishing dependence of corrosion on temperature gradient, it was also observed that the reaction depth of the Pd-SiC displayed the similar temperature gradient relationship [38]. The depth on the colder side was found to be much deeper than on the hotter side, ranging from 1 μm to 15 μm, with 5 μm being the median.

With regard to the occurrence of Pd in UO_2 kernels, it is has been found to exist as metallic inclusions with molybdenum, technetium, ruthenium and rhodium in the intact UO_2 coated particle. These inclusions occur mainly along the grain boundaries of UO_2 [42].

From a number of experimental analyses, Tiegs [41] was able to draw a conclusion that the irradiation temperature, kernel composition, palladium concentration, presence of other fission products and properties of the SiC layer, all contributed to corrosion of SiC by Pd. However, the irradiation temperature was found to be the primary cause of corrosion while others were of secondary importance. In addition, from a number of experiments, Minato *et al*. [38] were able to summarise the SiC corrosion mechanism by Pd by the following steps which are summarised diagrammatically in Fig. 2.9

1) birth of palladium by fission in the fuel kernel,

2) release of palladium from the fuel kernel,
3) transport of palladium to the SiC layer through PyC layers and
4) reaction of palladium with the SiC layers.

It has further been shown that the rate at which Pd-SiC occurs is determined by the slowest step of the above. For all UO_2 fuels, and thus for PBMR, it has been found that the slowest rate was Step 2, i.e. the release of palladium from fuel kernels. The birth rate of palladium and its amount depend on:
i) the burn up of the heavy metal,
ii) the density of kernel, and
iii) the volume of the kernel.

In the case of low enrichment fuels such those used in the PBMR, the contribution of ^{239}U in the increase of ^{239}Pu, which subsequently leads to an increase in palladium yield, increases with burn up since the fission yield of palladium from ^{239}Pu is much larger than it is from ^{235}U. This is because ^{239}Pu can be produced in the following two ways *viz.* a neutron reaction with ^{238}U which through a chain reaction ends up with ^{239}Pu and may be summarised by

$$n + {}^{238}_{92}U \rightarrow {}^{239}_{92}U \xrightarrow{\beta} {}^{239}_{93}Np \xrightarrow{\beta} {}^{239}_{94}Pu, \tag{2.9}$$

and also by an α-particle reaction with ^{235}U

$$\alpha + {}^{235}_{92}U \rightarrow {}^{239}_{94}U + \gamma\,. \tag{2.10}$$

Since the fuel is only enriched to 10% in ^{235}U, it implies that 90% of the fuel is ^{238}U and only 10% of this is ^{235}U, and also since ^{238}U can only undergo fission if reacting with fast neutron, which are in abundance in the reactor core, implies that it is a lot easier to produce ^{239}Pu from the ^{238}U reaction (Eq. (2.9)) than it is from $^{235}U(\alpha,\gamma)^{239}Pu$ reaction (Eq. (2.10)).

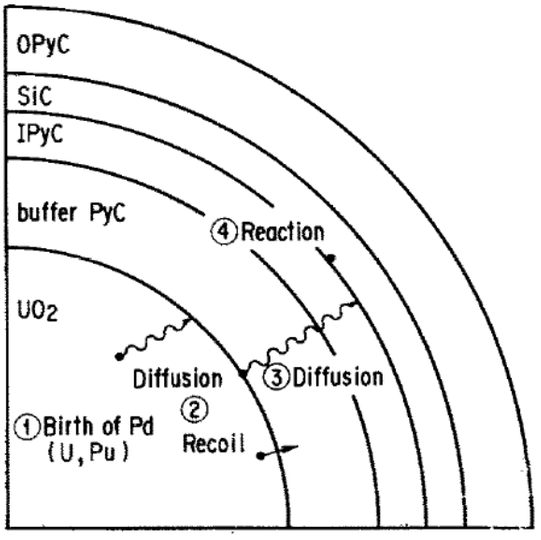

Figure 2.9: Schematic representation of interaction of palladium with silicon-carbide [38].

The half-lives of the precursor isotopes of palladium ^{105}Pd, ^{107}Pd, ^{108}Pd and ^{110}Pd (except ^{106}Pd), are all less than several tens of hours, which is negligible compared to the irradiation time [38, 43]. On the other hand, the half-life of ^{106}Ru, the precursor of ^{106}Pd is 369 days. Hence, the birth rate of palladium is also dependent on the irradiation time and period of the reactor shut-down.

Fission products may originate from anywhere in the fuel ranging from the surface of the kernel to the centre of the kernel. In order for the fission product to be released from the kernel two different mechanisms are utilised depending on the location where it was created. To be released and completely leave the kernel, those fission products which lie deep inside the kernel rely on a *diffusion* mechanism to migrate to the top surface of the kernel where they can escape the kernel, while those which are already on the surface of the kernel use a *recoil* mechanism.

Thus the release of palladium, which may be created anywhere from deep inside the kernel to top of the kernel, will be via either diffusion or fission recoil shown

in Fig. 2.9. The effective diffusion coefficient for palladium through to the surface is defined as [38]:

$$D_{\text{eff}} = \text{Bu}^{-1} \exp\ -Q/RT\ , \tag{2.11}$$

where

D_{eff} = the effective diffusion coefficient ($\text{cm}^2\ \text{s}^{-1}$),

Bu = the accumulated burn up (%FIMA),

Q = the activation energy (376 kJ mol^{-1}),

R = the gas constant (8.312 J $\text{mol}^{-1}\text{K}^{-1}$) and

T = the temperature.

The fractional release of palladium by recoil, F_{r}, may be defined as [38]

$$F_{\text{r}} = \frac{3}{4}\left(\frac{r}{a}\right) - \frac{1}{16}\left(\frac{r}{a}\right)^3, \tag{2.12}$$

where a is the radius of the fuel kernel and r is the recoil range, which has been estimated to be 8 μm.

The fractional release of palladium by diffusion, F_{d}, has been calculated from Booth diffusion model using the following equations [38, 50]:

$$F_{\text{d}} = 1 - \left\{ \sum_{i=1}^{k-1} \left[B_i\ \ 1 - F_r\ \ \ \tau_i g_i - \tau_{i+1} g_{i+1}\ \ / D_i^{'} \right] + B_k \Delta t_k g_k \right\} / \sum_{i=1}^{k} B_i \Delta t_i, \tag{2.13}$$

$$\tau = \sum_{j=i}^{k} D_j^{'} \Delta t_j, \tag{2.14}$$

$$g_i = g\ \ \tau_i\ \ = 1 - 4\sqrt{\tau_i/\pi} + 3\tau_i/2\ \ \text{for}\ \ \tau \le 0.1, \tag{2.15}$$

$$g_i = g\ \ \tau_i\ \ = \frac{1}{15\tau_i} - \frac{6}{\tau_i} \sum_{n=1}^{3} \frac{\exp\ -n^2\pi^2\tau_i}{n^4\pi^4}\ \ \text{for}\ \ \tau > 0.1, \tag{2.16}$$

$$D_i^{'} = \ D_{\text{eff}}/a^2\ \ = Bu_i^{-1} \exp\ -Q/RT_i\ \ / a^2, \tag{2.17}$$

where

F_d = fractional release by diffusion,

B_i = palladium birth rate during *i*'th step,

Δt_i = the time duration of the *i*'th step,

D_i = the reduced diffusion coefficient during the *i*'th step,

D_{eff} = the effective diffusion coefficient during the *i*'th step,

Bu_i = the accumulated burn up at the midpoint of the *i*'th time step and

T_i = the temperature during the *i*'th step.

Based on [38] the total amount of palladium released (R_{total}) is defined by:

$$R_{total}^{Pd} = F_r + F_d. \tag{2.18}$$

2.3.1.1.1 Investigation of corrosion by other researchers

Another important researcher who made an enormous contribution to the understanding of corrosion mechanism by metallic attack is Lauf who conducted a number of experiments using different samples by a view of determining the exact course of SiC corrosion and the mechanism by which it takes place [43]. In TRISO-coated particles containing rare-earth oxides such as La_2O_3 and Sm_2O_3, Lauf was able to observe some movement of lanthanum into the buffer pyrocarbon layer and the same distribution was observed for Sm_2O_3, but no attack on SiC could be confirmed by optical microscope on either of these. From this, Lauf observed that TRISO coated particles containing Mo-Ru-Rh-Pd alloy were extremely corroded, with the material deposited along the circumferential lines in SiC layers identified to be Ru and Rh mainly. In addition to this, it was also noticed that some Pd and Rh remained in the inner layer carbon, while some Ru and Rh reached the outer low-temperature isotropic (oLTI) pyrocarbon layer.

Turning to TRISO-coated particles containing UO_2 plus rare-earth oxides, Lauf observed some movement of heavy metals from the kernel into the inner pyrocarbon layers on the cold side of the particles from which he concluded that this must be from the migration of uranium, other than that, no damage to SiC was observed [43].

Regarding TRISO samples containing UO_2 plus Mo-Ru-Rh, Lauf observed that some SiC interactions occurred randomly in few particles. Again, further analysis could only identify Rh in the nodules within the SiC, while the white phase within the inner low temperature isotropic (iLTI) layer and at the iLTI-SiC interface, were both found to contain Ru and Rh.

In TRISO samples containing UO_2 plus Pd, Lauf noted a number of observations which are summarised as follows:

a) Localized attack was noted in all samples, especially on the cold side of the particles. The attack was characterised by partial penetration of the SiC layer, generally associated with build-up of Pd at the SiC-iLTI interface. Free Palladium or possibly an unidentified reaction product formed a nodule at the attack side and the areas were nearly always optically anisotropic.

b) Small bright specks which looked like palladium were observed some distance into the coating's thickness where normally no localized attack would occur.

c) Metallic spots which are believed to be palladium were seen distributed along the grain boundaries of the SiC's circumference

For TRISO coatings containing UO_2 plus Ag, experiment showed that Ag-doped particles exhibited the same interaction mode as seen in Pd-doped particles. There was greater penetration by Ag than by Pd, which is believed to be due to the following causes:

i) Silver melts at 960°C, it would therefore be expected that when annealed at temperatures between 1200°C and 1500°C that there would be a considerable amount of this element in the vapour phase, a considerably higher vapour pressure and the correspondingly higher degree of mobility of its atoms than would be the case with palladium which has the melting point of 1550°C when annealed under the same conditions.

ii) Silver-doped particles contained more free metals than palladium-doped particles did, which made attack/nucleation sites much larger and therefore easier to observe.

2.3.2 Interaction of SiC with CO in TRISO fuel particles

Carbon monoxide (CO) is one of the major factors that threaten the effectiveness of SiC layer as a barrier to fission product migration and as an effective pressure vessel of the coated particle. In UO_2 fuels such as those used in the PBMR, it is formed by the reaction between PyC layer that surrounds the fuel kernels and oxygen atoms liberated from heavy metal atoms by fission [40, 41]. Carbon dioxide (CO_2) also has a similar effect, but to a lesser extent than CO does. SiC is normally protected by IPyC from the corrosive effects of CO, however, in case of failure of the IPyC, CO will come into contact with SiC layer and then corrosion processes will be initiated. What is worth noting here is the fact that the corrosion morphology of SiC by CO is remarkably different from that of palladium and rare-earth elements; mechanical failure of IPyC as well as corrosion of the SiC layers occurs along the grain boundaries of the SiC. Small white precipitates are seen at the corroded area. The characteristics of the corrosion of SiC layer observed by Minato [41] at the Japan Material Test Reactor (JMTR) are as follows:

- The mechanical failure of the IPyC layer is often observed besides the area of the SiC corrosion.
- The corroded areas were not always on the hot side of the particle.
- The grain boundaries of SiC seemed to be selectively corroded during the early stages of corrosion.
- The IPyC and the SiC layers were often debonded from each other in particles with corroded SiC layers.

On further analysis using an electron microprobe, Minato [41] was able confirm that the SiC and IPyC were debonded from each other, and that there were white products observed between these layers, later revealing that they contained, silicon, cerium and barium oxides. This confirmed that the SiC layers are corroded by CO on the hot side of the particle.

2.3.2.1 Corrosion mechanism of SiC by carbon monoxide

Many theories have been developed to try to explain the nature of the interaction between SiC and CO. One of the most widely accepted theories is that proposed by Flowers, Horsley and Stansfield [41] which is based on thermodynamic analysis of SiC-C-SiO_2 system. A schematic representation of this process is illustrated in Fig. 2.10.

In order for SiC corrosion to occur, it is important that the IPyC layer must first fail and lose its functionality as a protective layer of SiC from CO, which often happens as a result of irradiation induced shrinkage. The performance of the IPyC layer is dependent on its quality as well as the irradiation conditions to which it is subjected. It is, therefore, not recommended to make an IPyC layer from a porous pyrocarbon as gas can diffuse with ease and result in the corrosion of the SiC by CO.

When CO interacts with the SiC layer it results in SiC being oxidized to form SiO_2(s) and C(s) with a high pressure of SiO(g), where (s) and (g) refer to solid and gaseous phases, respectively. Because of this, further growth of SiO_2(s) as a reaction product is minimized because the rate of vapour transport of SiO(g) from the corroded area to the cold side of the particle and kernel is much faster.The transported SiO (g) at the cold side of the particle reacts to form SiO_2(s) or more stable oxides such as those of Si, Ce and Ba depending on whether CeO_2(s) and BaO(s) have been transported out of the kernel.

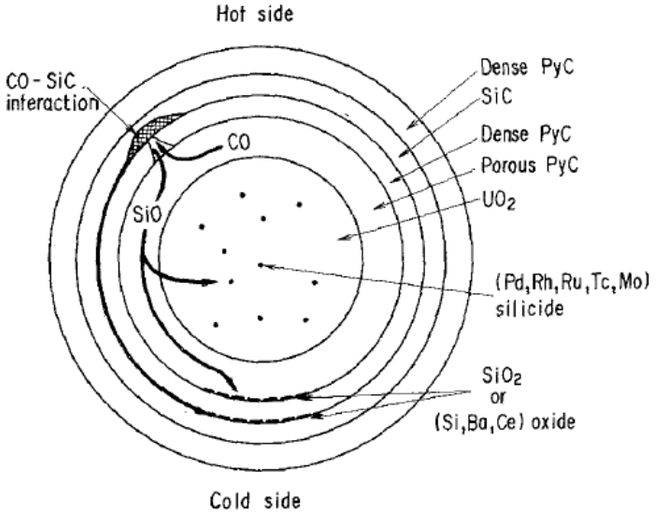

Figure 2.10: Schematic representation of corrosion of SiC by CO [41].

However, in the kernel, SiO(g) reacts with metallic inclusions to form stable silicides (Pd, Rh, Ru, Tc and Mo). As a result of these reactions, SiO_2(s) is not seen at the corroded SiC layer and CO is able to react with SiC directly. Hence, the formation of SiO_2(s) or oxides of Si, Ce, Ba results in the reduction of CO pressure in the coated particle and consequently in a longer life of the particle.

2.3.3 The role of internal gas pressure in fuel failure

The high operating temperature of TRISO fuel materials under normal and accident conditions makes it mandatory to understand the reactions (nuclear or chemical) that take place in UO_2 which could result in the fuel particle being damaged [20, 39, 44, 45, 46, 47]. The formation of oxides of carbon i.e. carbon monoxide (CO) and carbon dioxides (CO_2) at the fuel UO_2-buffer interface which leads to the build up of internal pressure was discussed in Section 2.3.2.1.

Among the critical factors that control the thermo-mechanical properties of the TRISO-coated particle is the internal pressure which results from the liberation of oxygen from UO_2 during the fission process and subsequent formation of CO(g) and CO_2(g) inside the coated particle [22] (see Section 2.3.4).

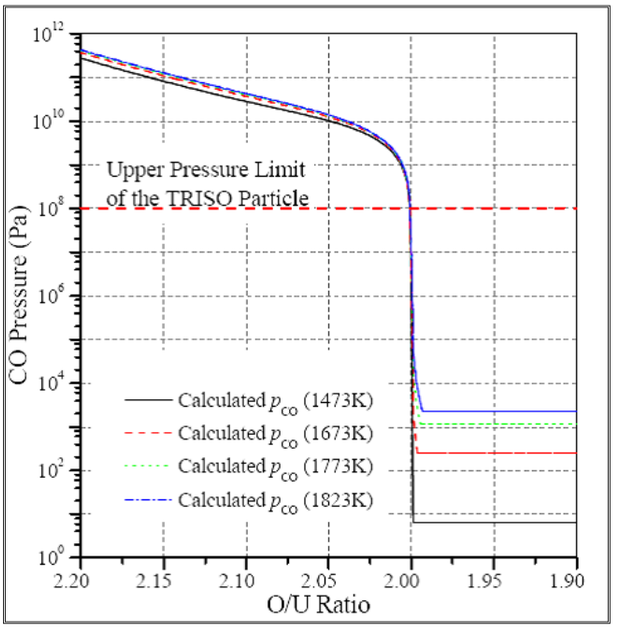

Figure 2.11: An illustrative diagram of partial pressure of carbon monoxide as a function of the ratio of O/U [48].

High pressures could lead to pressure vessel failure of the kernel. In this respect, it is critically important to understand all factors which can lead to an increase of this pressure and develop means to curb any further increase beyond the safety limit.

Gosse [48] reported that when the fuel temperatures reaches about 1000°C interaction between UO_2 and carbon to form gaseous oxides of carbon referred to above increases dramatically (See Fig. 2.11). A thermodynamic analysis conducted by Minalto *et al.* [40] indicated that the equilibrium pressure of CO(g) is higher than that of CO_2(g) and that the equilibrium pressure of these two species is highly dependent on the oxygen potential of the system, and thus the stoichiometry of the fuel $UO_{(2+x)}$. The correlation between stoichiometry of the fuel (O/U ratio) and the partial pressure has been studied extensively and is indicated in Fig. 2.11, from which it can be deduced that the upper limit of carbon monoxide internal pressure in UO_2 fuels is 100 MPa and should not under any circumstances be exceeded [48]. It should be noted that as long as the O/U ratio in the UO fuel remains below 2, the contribution of CO_2 can be neglected.

2.3.4 Scenarios for determination of internal gas pressure

Calculation of the internal pressure resulting from partial pressures of the fission gas products, CO(g) and CO_2(g) is one of the key elements of the pressure vessel failure analysis which is critical in providing an estimation of when the particle is likely to fail. The internal pressure acting on the dense coating of the coated particle is sum four main components:

- partial pressure of gaseous Fission Products (FP) (Xe, Kr, I, etc),
- partial pressure of CO (p_{CO})
- partial pressure of CO_2 (p_{CO_2}) and
- partial pressure of residual gas as a result of manufacturing processes.

At higher temperature, in addition to gaseous fission product like, Kr and Xe, some solid fission products (Cs, Rb, and Te) may also undergo sublimation and change from the solid to the gaseous state, as a result of this they contribute about 10% of pressure to the internal pressure of the coated particle. Their total pressure must be determined to determine if the Ultimate Tensile Strength (UTS) of SiC has not been exceeded. Because of the co-existence of the three states at the same temperature, the total pressure is thus calculated from the Redlich-Kwong equation of state using gas constants *a* and *b* listed in Table 2.1 [39, 50] rather than from the ideal gas equation. The Redlich-Kwong equation is defined as:

$$P_i = \left(\frac{RT}{V_i - b_i} \right) - \frac{a_i}{V_i \left(V_i + b_i \right) T^{1/2}}, \tag{2.19}$$

where

P_i = partial pressure (Pa) for gas *i*,

V_i = volume per moles ($m^{-3}\,mol^{-1}$) of gas *i*,

T = temperature (K) and

R = gas constant (8.31441 $J\,K^{-1}mol^{-1}$).

Table 2.1: Redlich-Kwong gas constants [22, 49].

Gas	T_c **(K)**	P_c **(MPa)**	a **($Nm^4K^{0.5}/mol^2$)**	b **(m^3/mol)**
CO	132.91	3.5	1.72	2.74×10^{-5}
CO_2	304.14	7.38	6.46	2.97×10^{-5}
Kr	209.45	5.5	3.411	2.74×10^{-5}
Xe	289.75	5.9	7.158	3.54×10^{-5}

The gas constants a_i and b_i have values that are found by acknowledging that at the critical point,

$$\left(\frac{\partial P}{\partial V}\right)_T = \left(\frac{\partial^2 P}{\partial V^2}\right)_T = 0 \tag{2.20}$$

and the values of a and b for each gas may be calculated from

$$a = \frac{R^2 T_c^{2.5}}{9\xi P_c} \tag{2.21}$$

and

$$b = \frac{\xi R T_c}{3P_c} \tag{2.22}$$

where T_c is the critical temperature, P_c is the critical pressure and ξ is a coefficient equal to $(2^{1/3}-1) \approx 0.259921$.

It has been shown that the fission-product partial pressure is dependent on burn up and the temperature. On the other hand, in addition to being influenced by irradiation temperature, burn up etc, the partial pressures of CO and of CO_2 are influenced by free oxygen (See fig. 2.12) which results from the fission of plutonium, and consequently in an increase of CO and CO_2. This is primarily because PBMR fuel is in the form of UO_2 and also contains small amounts of $PuO_{(2-x)}$ impurities.

Table 2.2: Comparison of amount of free-oxygen released per fission of heavy metal as a function of temperature.

Temperature (°C)	**Atoms of oxygen in one fission of ^{235}U (O/f_U)**	**Atoms of oxygen in one fission of ^{239}Pu (O/f_{Pu})**
1000	0.002	0.12
1200	0.0092	0.18
1400	0.031	0.23
1600	0.076	0.28

Studies conducted by Golubev *et al.*[82] and Proksch *et al.*[83] have shown that when these heavy elements undergo fission they release the oxygen atoms attached to them and that the oxygen released from UO_2 is removed through oxidation processes while that from $PuO_{(2-x)}$ is not. It is this excess oxygen produced in the fission of Pu that available as free-oxygen that is responsible high levels of CO and an increase in P_{CO}. Not only did these studies show that fission of ^{239}Pu results in higher amounts of free-oxygen than fission of ^{235}U, they also showed that the amount of free-oxygen is also dependent on the fuel temperature as shown in Table 2.2. The mathematical relationship between fission of Pu and production of free-oxygen from low enriched fuel (^{235}U < 20%wt) as a function of temperature is based on the model derived by Homan [22]:

$$\frac{\mathrm{O}}{f_{\mathrm{Pu}}} = 1.64 \exp\left(-\frac{3311}{T}\right) \tag{2.23}$$

and

$$\frac{\mathrm{O}}{f_{\max}} = 0.61, \tag{2.24}$$

where O/f_{max} is the maximum atomic oxygen release per fission and T is the temperature (K). Golubev *et al*. were also able to prove that production of CO_2 is negligible compared to that of CO.

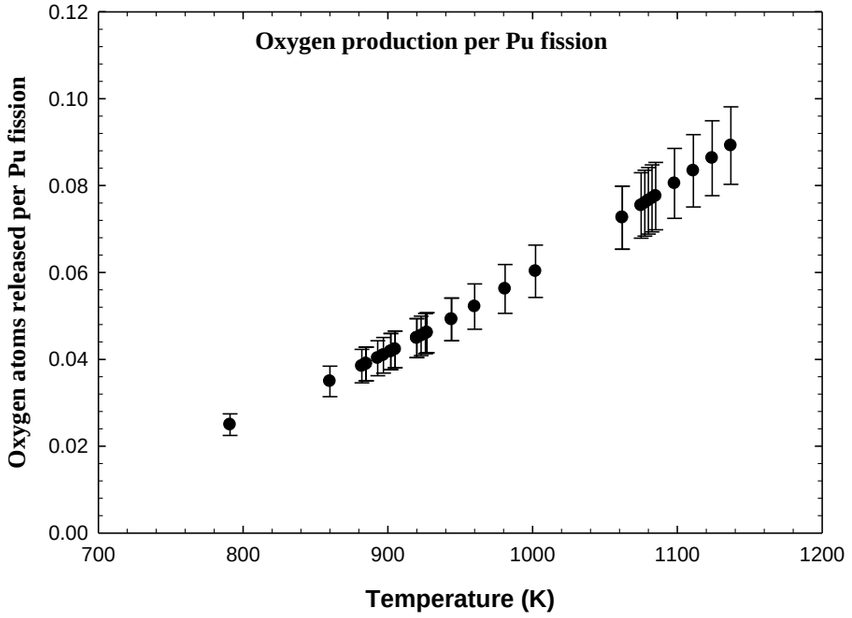

Figure 2.12: Atomic oxygen released per fission of plutonium (present study).

The graphical relationship between oxygen atoms released from the HFR-K5 sample *versus* the temperature has been found to fit Eq. (2.23) is illustrated in Fig. 2.12, and concurs with the research findings obtained by Snead *et al*. [29].

2.3.4.1 Pressure Vessel failure scenario

The structural integrity of the TRISO-coated fuel particle is measured by the tangential stress at the inner surface of the SiC layer. When this stress exceeds the fracture strength of the SiC, the particle will fail [20]. It is, therefore, important that the total stress, δ, resulting from internal pressures does not exceed the Ultimate Tensile Strength (UTS) of the TRISO coated particle. The TRISO Pressure Vessel Model [20] is the most widely accepted model able to describe this phenomenon.

The essential feature of the TRISO Pressure Vessel Model considers the fuel particle as a thick-walled elastic vessel with gaseous fission products exerting a

continuously increasing internal pressure as the kernel burn-up increases, where the pressure is dependent on the available void volume, which in turn is a function of the density and dimensions of individual phases and the number of fissions. Thus, the basic assumptions as reported in Kovac's study [20] which need to be accepted as a starting point before the use of the Pressure Vessel Model are:

- the vessel is a spherical, thick-walled structure with the maximum tangential tensile stress occurring at the inner SiC surface;
- void volume for fission gases is available in the kernel and buffer;
- gases contributing to the internal gas pressure are long-lived Xe and Kr, and the oxides of carbon CO and CO_2;
- void volume in the particle is reduced during burn up as a consequence of low-density metallic products.

The Pressure Vessel performance of a TRISO fuel Particle is divided into two main categories.

Category I

Failure in this category is characterised by a load-bearing SiC layer that is capable of sustaining a high tensile-stress component. The TRISO particle failure will occur when the SiC fracture strength is exceeded, which results in an instantaneous release of elastic energy enough to cause simultaneous failure of the pyrocarbon layers. The underlying assumption for this failure mode is that the strength of the OPyC layer is insufficient to accommodate the strain energy released at the onset of SiC failure; consequently, the TRISO particle undergoes a catastrophic bursting-type failure, which is also known as "Classical Pressure Vessel Failure" [20].

Category II

Failure mode in this category is characterised by a defective SiC layer which is incapable of bearing a tensile stress. The pyrocarbon layers are a structural support containing internal fission-gas pressure. The defective SiC layers created during particle coating or during the manufacturing process are all classed as

manufacturing defects, and the SiC layers which are structurally degraded as a result of metallic fission product attack or kernel migration are classified as irradiation-induced defective SiC layers. Both classes of defective SiC layers are treated under Category II failure mode. Failure in this category is sometimes termed “Defective SiC Pressure Vessel Failure” [20].

Although these two categories are distinctively different from each other, there are remarkably common underlying features in treating both of them; namely, the maximum stress in the load-bearing component of any particle is dependent on the dimensions and densities of individual phases plus the temperature, burn up and the fluence to which the particle is subjected.

The classical pressure vessel failure (Category I) is calculated by allowing the SiC layer to bear a tensile stress component and comparing the tensile stress to a randomly selected fracture strength. In contrast, defective SiC (Category II) pressure vessel failure is based on calculating Inner Pyrolytic Carbon (IPyC) and Outer Pyrolytic Carbon (OPyC) stresses at the moment the SiC stress changes from compressive to tensile i.e. a condition of zero stress. The pyrocarbon stresses are then compared with their fracture strengths, and particle failure occurs when both the IPyC and OPyC have failed. To prevent any of the failure mechanism from taking place, it is recommended that the following rule of thumb is heeded at all times [20, 22]:

$$\begin{aligned} &P_{\mathrm{CO}} < 100 \text{ MPa} \\ &P_{\mathrm{CO}} + P_{\mathrm{Xe}} + P_{\mathrm{Kr}} + P_{\mathrm{CO_2}} + P_{\mathrm{I}} .... < 350 \text{ MPa}. \end{aligned} \tag{2.25}$$

2.3.5 Yield of gaseous fission products and other associated gasses

Xe and Kr are the primary gas fission products resulting directly from the fission process. However, there are other gasses which are generated as by-products of chemical reaction between various layers of the TRISO coated particle. Some of these include O_2 which is produced whenever plutonium undergoes fission

process which in turn reacts with the carbon of SiC to produce CO_2. The number of moles of fission gases produced inside the fuel kernel may be calculated using the following equation taken from Kovacs *et al*. [20]:

$$M_{\mathrm{Kr/Xe}} = M_{\mathrm{K}} \times \mathrm{FIMA} \times \mathrm{FY}_{\mathrm{Kr/Xe}}, \tag{2.26}$$

where

$M_{\mathrm{Kr/Xe}}$ = number of moles of Krypton or Xenon produced

FIMA = fraction initial heavy metal atoms fissioned

$\mathrm{FY}_{\mathrm{Kr/Xe}}$ = fission yield of Krypton or Xenon

M_{K} = number of moles of metal atom in kernel.

Here, M_{K} depends on the kernel radius, a random variable, and is defined as:

$$M_{\mathrm{K}} = \frac{4}{3}\pi r_{\mathrm{K}}^3 \times \rho_{\mathrm{K}} \times \frac{\overline{W}}{M_w}, \tag{2.27}$$

where r_{K} is the kernel radius, ρ_{K} is the kernel density, $\overline{W}$ is the weight fraction of metal in kernel and M_{W} is the molecular weight of metal in kernel.

The amount of CO(g) produced from the OU_2 fuel as a result of reaction of oxygen with carbon may be calculated as follows [20]:

$$M_{\mathrm{CO}} = M_{\mathrm{K}} \times FIMA \times \frac{O}{F}. \tag{2.28}$$

In contrast to CO, very little CO_2 is produced under normal operating conditions of the HGTR. The total internal gas pressure is as described in Section 2.3.4. In addition to the expansion, the IPyC and OPyC layers in TRISO coated particles undergo quite a significant amount of irradiation-induced shrinkage as a result of fast fluence exposure. Consequently, the OPyC places a huge amount of compressive stress on the SiC, which counteracts the SiC tensile stress induced by internal gas pressure. The IPyC, on the other hand, acts in a way that tends to reduce the SiC tensile stress by tending to contract while maintaining contact with inner SiC surface. Thus, the effect of IPyC on the SiC tensile stress is negated by assuming 100% failure fraction of IPyC, a position which is supported by results of several post-irradiation tests.

2.4 Modes of TRISO-coated particle failure

The particle may undergo several modes of failure, each with its own characteristics. However, there are only two which have been well studied and the mechanism of failure recorded and are described the next two sections.

2.4.1 Category I failure mode

This failure mode occurs when the maximum tensile stress in SiC layers exceeds the fracture strength of that SiC layer. The stress and fracture strength are independent random variables, and particle failure occurs when [20]

$$\sigma_{\mathrm{SiC}}^{\max} \geq \sigma_{\mathrm{F}} \quad \mathrm{SiC} \ , \tag{2.29}$$

where the F subscript indicates that it is the fracture strength that is being referred to.

2.4.2 Category II failure mode

This often occurs when the maximum tensile stresses in the pyrocarbon layers exceed the fracture strengths of these layers. When both of the IPyC and OPyC layers are intact the two pyrocarbon layers bear the internal gas pressure jointly, which results in the reduction of the tensile stresses in each one of them. After failure of either of the layers, the remaining layer bears the entire load on its own which if not strong enough will burst. Thus, both of these layers, IPyC and OPyC must fail before total particle failure can occur. The PyC failure conditions in the model are expressed mathematically as follows [20]:

$$\begin{aligned} \sigma_{\mathrm{IPyC}}^{\max} &\geq \sigma_{\mathrm{F}} \quad \mathrm{IPyC} \\ \sigma_{\mathrm{OPyC}}^{\max} &\geq \sigma_{\mathrm{F}} \quad \mathrm{OPyC} \ . \end{aligned} \tag{2.30}$$

Fracture strength is not an intrinsic feature of any given material, its estimations needs a probabilistic approach. The widely accepted approach is that of the Weibull Theory [20], which presupposes that:

- the solid is statistically homogeneous;
- the fracture of the least resistant element causes the total collapse of the fracture.

From these principles, the cumulative failure probability of SiC is given by the following conventional expression [22]:

$$P_{\mathrm{R}} = 1 - \exp\left[- \int_{D} \left(\frac{\sigma \ x, y, z}{\sigma_{0\mathrm{D}}} \right)^{m} dD \right], \tag{2.31}$$

where D is a dimension (volume or surface), σ is the tensile stress dependent on the location (x,y,z) and m is the Weibull modulus and is calculated from

$$m = 8.02 - 0.425\Phi, \tag{2.32}$$

where Φ is neutron fluence in 10^{25} n/m^2 and $\sigma_{0\mathrm{D}}$ is the characteristic strength.

2.5 Diffusion of fission products through the TRISO coated particle layers

Diffusion is an important aspect of how fission products migrate through various layers of the TRISO coated particle and how they are eventually released. Therefore, understanding how diffusion occurs in SiC is of critical importance. Diffusion is governed by two fundamental factors which were derived by Fick in 1880 and apply to any state of matter due to the general character regarding macroscopic diffusion processes [23, 24, 33].

Although there are many different modes of diffusion that can take place in a solid solution like SiC, depending on temperature conditions, they all use the same elementary principles of a jump of an atom from one stable position of a crystal lattice to another. While some may require the presence of defect such as vacancies, others will do better in the presence of interstitial atoms instead.

2.5.1 Vacancy diffusion mechanism

Vacancy diffusion mechanism relies on the availability of a vacancy into which an atom may jump from its lattice site to a neighbouring vacant site for diffusion to occur [28, 33, 42, 51]. As the atom moves towards a vacant lattice site, it leaves behind a vacant site which it previously occupied, which is also almost immediately occupied by the next atom etc. Thus, whenever an atom makes a move in one direction, the vacancy makes an equal but opposite movement. Vacancy-type diffusion is the number of jumps per unit time of either the atom or the vacancy, which is proportional to *z*, the number of vacant sites, because the vacancy will only jump to the nearest neighbour if that site is vacant. This process is illustrated in Fig 2.13. Hence, the diffusion coefficient for atomic diffusion (which only considers diffusion of atoms and not those of vacancies) is given by [33]:

$$D_a^v = 1/6z\lambda^2\ p_v\omega, \tag{2.33}$$

where p_v is the probability that a given neighbouring site will be vacant when needed, ω is the frequency with which an atom jumps to a particular site and λ is jump distance. The overall diffusion coefficient which accounts for atomic as well as vacancy diffusion is given by

$$D_v = \alpha a^2 \omega, \tag{2.34}$$

where

$$\alpha = 1/6zA^2, \tag{2.35}$$

and the jump distance λ is related to the lattice constant *a* (illustrated in Fig. 2.6) by $\lambda = Aa$ and *A* is coefficient that depends on the type of diffusion mechanism and the type of crystal structure of the material under consideration.

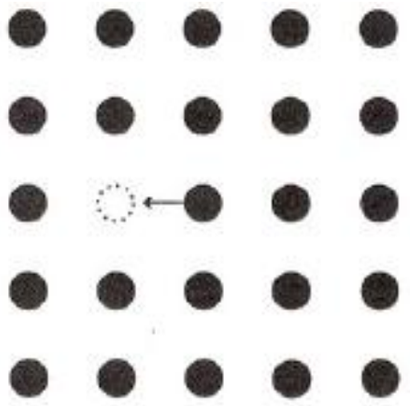

Figure. 2.13: A schematic illustration of vacancy diffusion mechanism [33]

2.5.2 Interstitial diffusion mechanism

This mechanism involves the movement of an atom from one interstitial position to another as illustrated in Fig. 2.14. A considerable amount of energy in the form of thermal vibration at very high frequency is required in order to overcome the energy barrier separating the adjacent interstitial sites and to push its way through the crystal. This diffusion mechanism will only occur when the atoms of the diffusing species are smaller compared to those of a host species, a criterion known as the relative size factor, which is one of the four critical factors that determine the diffusivity of one atoms of material by another. The other three factors are:

- **Crystal structure factor:** both Kr and Xe are FCC in structure, hence neither of them will have an advantage over the other in the diffusion through the SiC [23, 24].
- **Relative valence factor:** both Kr and Xe are noble gasses and thus have the same number of valence electrons. Thus, again neither of them will have an advantage over the other in diffusing through the SiC [23, 24].
- **Chemical affinity factor:** because of the similarity of the above two factors, chemical affinity is also the same since it is influenced by the two factors above.

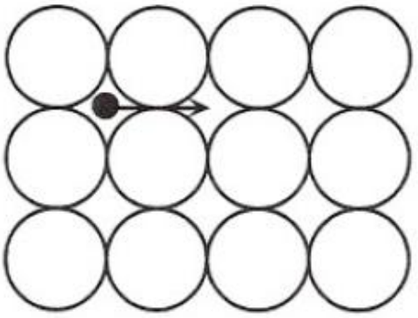

Figure 2.14: A schematic illustration of the interstitial diffusion mechanism [33].

For example, one can deduce from the Periodic Table that, of the dominant gaseous fission product encountered thus far, *Kr has smaller atomic radius compared to that of Xe primarily because Xe has one additional energy level more than Kr*.

Hence, since the other three factors referred above are all constant for both Kr and Xe, *it can be concluded that the relative size factor is the only factor among the four that determines the relative diffusion rates of these fission products in SiC*. Thus, because of this, Kr stands a much better chance of diffusing by interstitial mechanism than is the case with Xe, and will be confirmed later by Fig. 3.11.

2.6 Fission product release models

Fission product behaviour under high temperature and radiation conditions is of great interest to High Temperature Gas Cooled Reactors (HTGR) fuel scientists because of the effects of this environment on the TRISO fuel particles. Extensive research, see for example [22, 43, 44, 49, 51, 52, 56, 74], has been conducted to determine the interrelation between these factors, and the Booth model [21, 22, 52] has been widely accepted as the most realistic model to describe the fission product migration through the TRISO fuel. The fractional release is defined as [49]

$$F = 1 - \frac{6}{D't}\sum_{n=1}^{\infty}\frac{1-e^{-n^2\pi^2 D't}}{n^4\pi^4}, \tag{2.36}$$

where t is the irradiation time (s), D' is the reduced diffusion coefficient (s^{-1}), defined by $D' = D/r^2$ where D is the diffusion coefficient ($m^2 s^{-1}$) and r, is the kernel radius (m). The Booth model is very accurate in determining the ratio of the release rate to the birth rate *(R/B)* which depends on diffusion coefficient and decay constant of the fission product [49].

There are a number of variations of the Booth model, which differ only slightly, but in principle are the same [8, 49, 51, 52]. The differences lie in the type of fuel used and mainly whether the fuel is single crystalline or polycrystalline UO_2 [52]. The Booth model is widely accepted for use in single and polycrystalline UO_2 and is defined by:

$$R/B = \frac{S}{V}\sqrt{\frac{D}{\lambda}}$$
$$D = AF + B\sqrt{F}\exp\left(-Q_v/RT\right) + D_o \exp\left(-Q_I/RT\right), \quad (2.37)$$

where

S/V = surface to volume ratio of UO_2 (mm^{-1})

D = diffusion Coefficient of fission gasses in UO_2 ($m^2\ s^{-1}$)

λ = nuclides decay constant (s^{-1})

A = constant for athermal diffusion in oxide fuels (m^5)

F = fission rate density ($m^{-3}\ s^{-1}$)

B = constant ($m^3\ (m\ s^{-1})^{0.5}$)

Q_v = activation energy related to vacancy diffusion (J/mol)

D_o = constant ($m^2\ s^{-1}$)

Q_I = activation energy related to interstitial diffusion (J/mol)

R = Gas constant = 8.314 J/mol/K

T = temperature (K).

For each gaseous fission product (Kr and Xe) the values of the parameters of Eq. (2.37) are given in Table 2.2. From this it can be seen that for calculation of D, all constants will have the same values for both Xe and Kr except for F which is unique for each gas, and are all indicated in Table 2.2. However, for the calculation of *R/B* every nuclide has its own λ, *S/V* and D as calculated previously.

Table 2.3: Constants for the diffusion of gaseous fission products through the TRISO coated particle [50].

Parameter	Value
A	$2\text{x}10^{-40}\ \text{m}^5$
B	$1.41\text{x}10^{-25}\ \text{m}^2(\text{m/s})^{0.5}$
Q_v	115 kJ/mol
D_o	$7.6\text{x}10^{-10}\ \text{m}^2/\text{s}$
Q_I	293 kJ/mol
R	8.314 J/(molK)

In Germany extensive studies have been conducted on fission product release models because of their experience with AVR, as such a number of release models have been developed. One such model is that of Röllig developed in 2001 for release due to contamination which is given by [22, 50, 53, 56, 57]

$$\begin{aligned} D'_{\text{Kr}} &= 3.0\times10^{-5}\exp\left[-1.06\times10^{5}/8.314T\right] \\ D'_{\text{Xe}} &= 1.7\times10^{-7}\exp\left[-7.86\times10^{4}/8.314T\right]. \end{aligned} \tag{2.38}$$

Release due to fuel failure, D'_{f}, is based on the work by Nabielek and is defined as

$$D'_{\text{f}} = \left(\frac{500}{d}\right)^2 \times 10^{\,-2.6-\,8220/T}\ , \tag{2.39}$$

where d is the kernel diameter [22]**.**

Having given the necessary theoretical background to fission product release, it is now necessary to turn to experimental layout that was used and the detection of fission product release as a result of irradiation. All this together with the analysis of experimental results will be discussed in the next chapter.

CHAPTER 3

Experimental Investigation and Analysis

In order to preview the behaviour of coated particles under operating conditions of PBMR, the fuel samples were subjected to intensive radiation tests at HFR at Petten where the PBMR's operating conditions were simulated, and the irradiation test results submitted by to PBMR (Pty) Ltd for further analysis, which is the basis of this Research Report [81]. The results were analysed for fission products released and dimensional changes that occur as a result of the effects of radiation. The experimental layout and the analysis of the results will be described in detail in this chapter and the findings will be presented in Chapter 4**.**

3.1 Description of the HFR Materials Testing Research Facility at Petten in The Netherlands

The High Flux Reactor (HFR) situated at Petten in The Netherlands is a 45 MW_{th} multipurpose materials testing Light Water Reactor (LWR) of the tank-in-pool type [21]. It is operated on a schedule of 11 or 12 cycles per year, with each cycle consisting about 25 operating days and 3 shutdown days. It consists of twelve horizontal beam tubes which are used for neutron research, thus providing the researcher with a variety of irradiation possibilities, such as in the reactor core, the reflector region as well as in the poolside facility outside the reactor [21]. The fission gas released from the TRISO-coated fuel particles during the irradiation process, which serves as an indication of the degree of fuel damage, is detected using the experimental layout and detection system described in Fig. 3.1.

3.1.1 Sample Holder

The HFR sample holder is made up of three main sections; lower, middle and upper sections, which are tightly fixed together with bars.

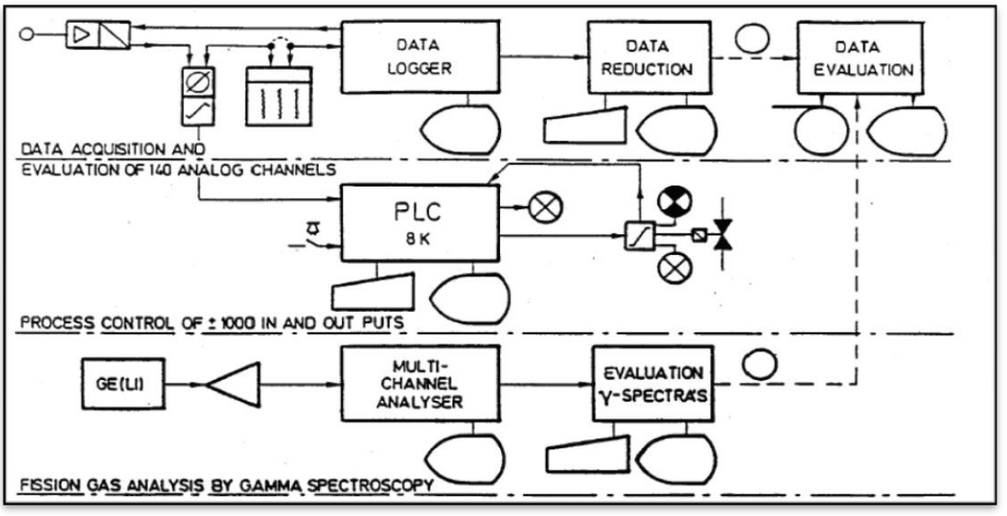

Figure. 3.1: Fuel failure detection system [21].

Four samples are irradiated at any given time, and the samples are loaded as follows: 1 each in upper and lower sections and 2 in the middle section, as illustrated in Fig. 3.2.

3.1.1.1 Irradiation rig

The pebbles and the graphite half-shells are enclosed in a stainless steel capsule whose material properties have been tested and verified to be able to withstand the radiation damage which could result from high neutron flux, and the capsule material does not release any impurities as this could potentially affect the results of the experiments [21]. The instrumentations used for the detection of released gas, Fig 3.1, also regulate the flow rate of helium (He) gas into Reactor Pressure Vessel (RPV) where it serves as a cooling medium and as well as the inert environment under which irradiation takes place. The helium-gas supply tubes penetrate the sample-holder cap from the top, and the penetrations are sealed by means of high temperature brazing to prevent convective heat loss.

The heat generated by gamma absorption and nuclear fission is dissipated radially by conduction through the test material, thus ensuring an even heat distribution throughout the test sample, and also through the gas caps by conduction and

radiation to the outside containment. Because of the heat generated from the irradiation process, the Reactor Pressure Vessel (RPV) gets very hot, and thus is cooled down by a stream of contra-flow of primary cooling water.

(i) Middle section

The middle section is made up of shielding plugs, dust filters on all capillary tubes and activated charcoal filters. One filter containing activated charcoal is situated on the down-stream side of the second containment in order to absorb any radioactive gas that might be released in this containment.

(ii) Upper section

The upper section is made up of a penetration plug with the dynamic O-ring sealing of the thimbles and connectors for the thermocouples, connectors for the gas lines and a Visual Display Unit (VDU) situated in the rig head as well as three solenoid valves. The main purpose of dynamic sealing is to ensure leak tightness to ensure no radiation leaks takes place during operation of the reactor. The valves are used to isolate the capsule so that if the purge gas has to be routed elsewhere, it should be possible to do so easily, and so that during maintenance operations the capsule can be isolated from the rest of the plant.

3.1.2 Instrumentation

A number of instruments are used in the entire fission product detection system. They are categorised into two groups namely, the process instrumentation and nuclear instrumentation and are discussed in detail below.

3.1.2.1 Process instrumentation

The primary purpose of these instruments is to measure and regulate the sample's surface and central temperature since they play a significant role in fission-product release rate and, therefore, need to be monitored carefully. Bakker *et al*. [21] comment that the temperature data are recorded in the data logger of the central HFR computer data acquisition system (DACOS), and that one of the most

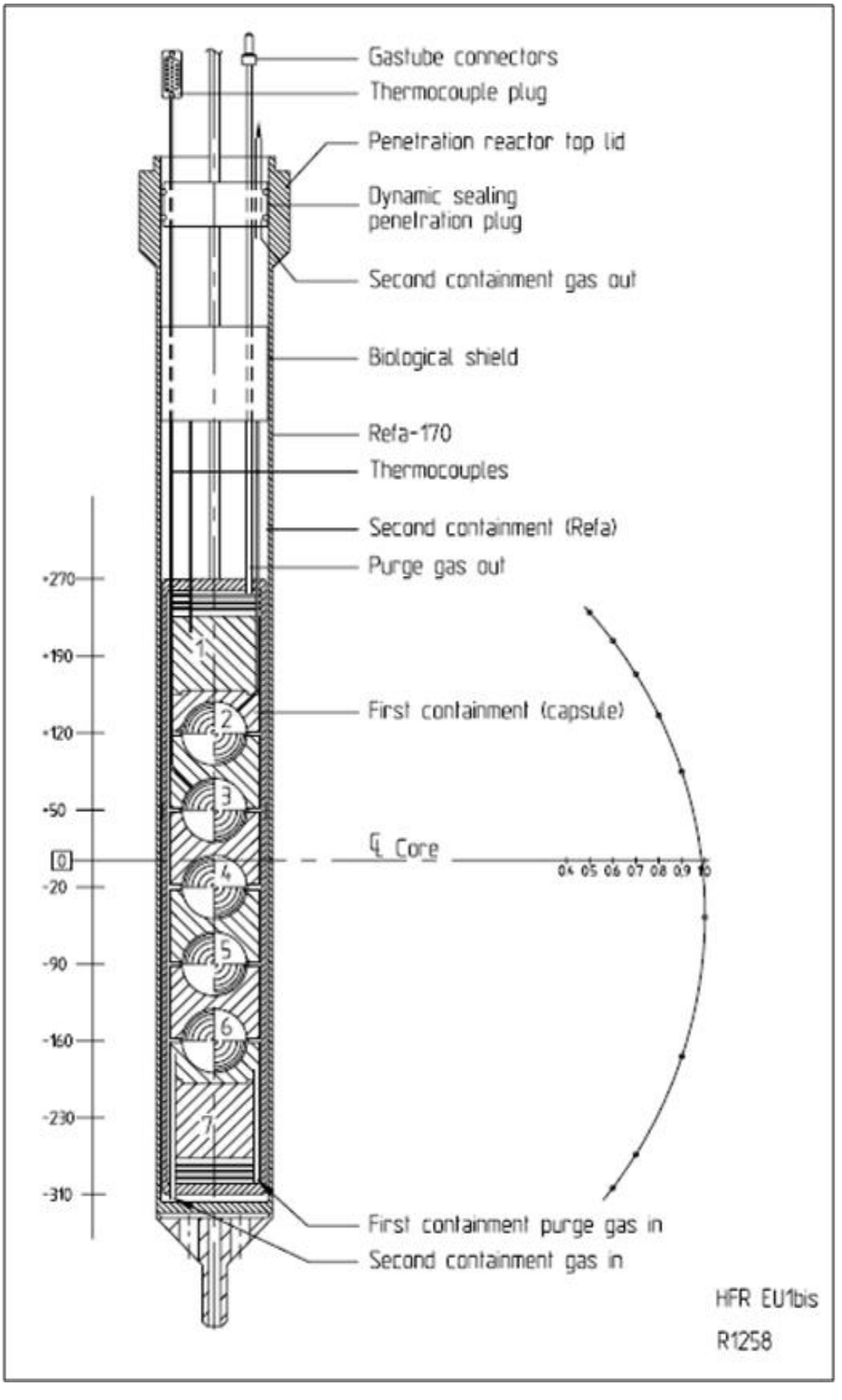

Figure. 3.2: Sample holder used at the HFR Material Testing Facility at Petten, The Netherlands [21].

important functions of the process instrumentation is to regulate the flow rate of the inert gas to sweep through the containment at a constant rate so as to provide an inert environment under which irradiation is conducted as well to act as coolant.

3.1.2.2 Nuclear instrumentation

The HFR is equipped with a number of nuclear instruments that are important in neutron dosimetry. These include among others: 2 Geiger Muller counters, 24 thermocouples, 3 standard neutron fluence detectors (FDs) positioned between pebble test samples in the graphite half-shells providing valuable information on the accumulated fluence after the experiment and a Gamma Scan Wire (GSW) situated inside the central tube of the sample holder. The GSW is made up of 1 mm diameter stainless steel which extends the entire length of the capsule. After the irradiation, the neutron detectors and GSW are analysed by means of gamma spectroscopy for:

1. Thermal neutron fluence,
2. Fast neutron fluence,
3. Fuel burn up,
4. Equivalent fission fluence,
5. Spectrum indices and,
6. Axial and Azimuthal relative and absolute distribution of thermal and fast fluence.

Other scientific instruments include the temperature, gas analysis data and γ-spectrometer. Gamma spectroscopy is a non-destructive method of measuring the relative distribution of fission products in irradiated fuel pebbles. To obtain the necessary information, complete γ-ray spectra are accumulated as a function of axial and transversal position. The net area under full-energy peaks is determined, giving quantitative measurements of the amount of each radioactive fission product. The instrumentation for γ-spectroscopy is made up of:

- Ge(Li) Detector
- Multichannel Analyser

- Gamma spectra display.

The experimental layout of these instruments to effect γ-detection is indicated in Fig. 3.1. The gas analysis is performed by regular sampling in the gas panel after bypassing the first containment filters.

3.1.3 Test samples and irradiation conditions

The samples irradiated consisted of four TRISO coated pebbles made to the German standard. The A1K5 sample was irradiated at HFR at Petten in the Netherlands as a proof test for HTR MODUL, but analysis of fission product release was left to PBMR Pty (Ltd) fuel scientists to develop their fission product analysis skills, which is the subject of this Research Report. Other samples were reserved for irradiation at the SAFARI reactor with the view to validating the PBMR fuel qualification programme as well as determining the ability of the SAFARI reactor to reproduce irradiation tests that are comparable to other similar material test facilities e.g. HFR. The sample under investigation was A1K5 and its composition and irradiation parameters are given in Table 3.1.

The sample was located in various reactor test positions to mimic the expected PBMR reactor operating conditions so as to determine the neutron flux that has the greatest effect on the lifespan of the sample. This was done taking into consideration that the flux map may change during operation of the reactor. The irradiation position of the samples with respect to the test reactor core is illustrated in Fig. 3.3. It is particularly important that the irradiation position of the sample is known since the flux density is not uniform throughout the RPV.

3.2 Effects of irradiation of TRISO coated particle.

The harsh environmental conditions to which the PBMR fuel element is subjected to as a result of high operating temperature and neutron fluence often results in dimensional change of the fuel sphere and the TRISO coated particle. The degree of dimensional change depends on the extent of exposure. The amount of influence on dimensional change as a function of neutron dose, temperature and

Table 3.1: HFR K5 sample specification [8].

Parameter	**Units**	**Fuel Element Designation**				
		A1K5	B1K5	B2K5	C1K5	PBMR
		Specification				
Fuel Element no	Serial no	2953-12	2953-42	2953-68	2953-72	-
Uranium content	g	9.44	9.44	9.44	9.44	9.00
^{235}U enrichment	%	10.7	10.7	10.7	10.7	9.6
CP [2content		14600	14600	14600	14600	14500
Failed CP content	Per FE[3	0	0	0	1	0.4
		Irradiation data				
Burn up (FIMA)	%	7.9	10.2	10.5	9.4	9.8
Neutron Fluence (> 0.1 MeV)	10^{21} cm^{-2}	2.9	4.0	4.3	3.9	2.7
Max Centre Temperature	°C	1020	1070	1010	1030	1040
Max Power Output	kW/FE[2	2.21	3.03	3.03	3.19	3.06

[2 CP = Coated Particle
[3 FE = Fuel Element

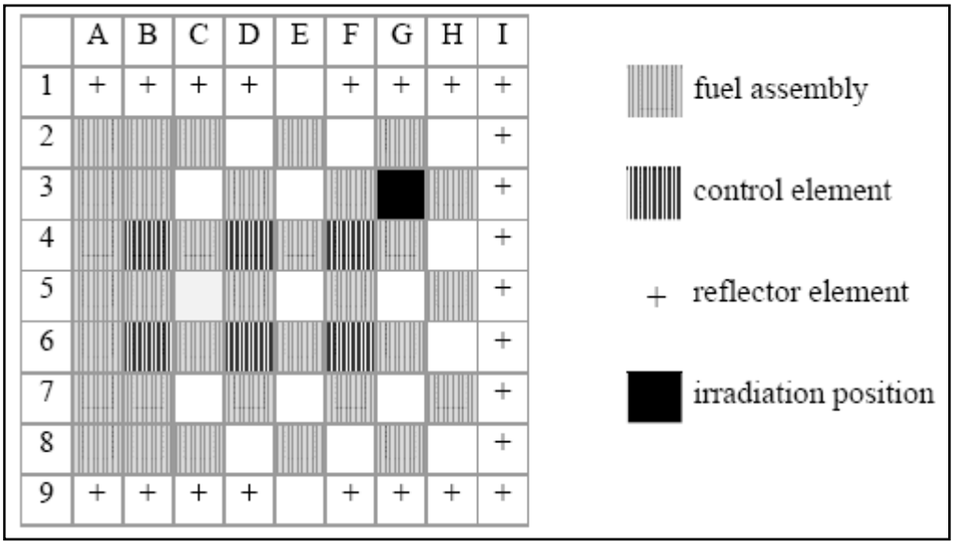

Figure 3.3: Core configuration of the HFR Material Testing Research Facility at Petten, The Netherlands, illustrating sample irradiation position [21].

duration of exposure change was investigated in detail and will be discussed in the following sections.

3.2.1 Fuel swelling and/or shrinkage

Neutron reaction with fissile material yields a number of gasses, ranging from gaseous fission products (Xe, I and Kr), CO (g) and CO_2 (g) which expand when the temperature increases [28, 53-56]. Because of this they exert an enormous amount of pressure against the SiC inside the kernel and force the coated particle to expand accordingly. Snead *et al*. [29] have been able to prove that the relationship between coefficient of thermal expansion and temperature is given by equation (3.1). In the irradiation experiment, the temperature of the coated particle was recorded and because it is related to the coefficient for thermal expansion a plot of temperature *versus* α as determined from Eq. (3.1) yields a correlation indicated in Fig. 3.4. This is the reason why the coefficient of thermal expansion, α, for the coated particle shown in Fig. 3.4 increases as the temperature increases.

$$\alpha = -1.8276 + 0.0178T - 1.5544\times10^{-5}T^2 + 4.5246\times10^{-9}T^3 \ (10^{-6}/\mathrm{K}) \qquad (3.1)$$

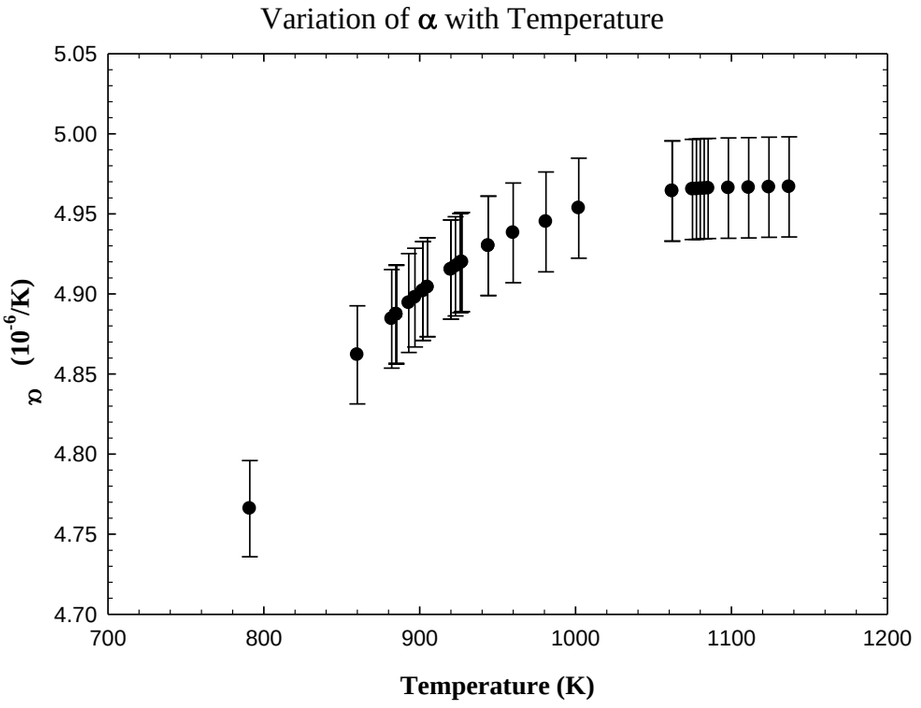

Figure 3.4: Coefficient of thermal expansion, α, of SiC (present study).

This has been found to be in agreement with studies conducted by other researchers [22, 29].

In material exposed to high neutron fluxes, the neutrons knock atoms away from their matrix positions, generating vacancy-interstitial pairs and also creating helium by transmutation. Through the formation of immobile structures and preferential absorption of microstructures, a super-saturation of vacancies is formed within the material. With the aid of helium as the nucleation site, the excess vacancy coalesces into bubbles and after further accumulation of vacancies grow into voids, as a result of which swelling occurs. This is of particular importance to fuel designers as a screening method for Low-Enriched Uranium (LEU) to be accepted as fuel or not. Previous studies by Dubinko and Kemp [54, 57] and Rest *et al.* [59] reported that a void-driven growth mechanism results in swelling which is significantly higher than that driven by bubbles and often leads to a breakaway swelling behaviour. That is the reason why the graph of volume

versus irradiation time in Fig 3.5 shows two dimensional-change regions, one below 0% and the other above 0%. For detailed discussion on this, refer to Section 3.2.2.

It has been shown that bias driven swelling of the kernel is as a result of swelling of solid fission products such Cs, Ag and Sr [33]. This has an advantage that when such swelling occurs the interstitial spaces between silicon and carbon atoms of SiC are blocked, thus preventing other impurities which might have a much higher coefficient of thermal expansion from occupying the interstitial spaces, resulting in much bigger volumes and subsequent increased swelling of the coated particle. Another factor that contributes to swelling of the kernel is due to expansion of the gaseous fission products liberated in the kernel which results mainly in the increase of the bubble and void population.

3.2.2 Effect of duration of irradiation on volume change

When all other factors are kept constant, the volume change as a function time indicates that there is sharp increase in volume change during the first few weeks of irradiation, reaching a maximum of 0.2% increase in about 50 days, and will be confirmed later in Fig. 3.5. Note that the duration of irradiation is measured in Effective Full Power Days (EFPD). Further irradiation beyond that results in a second steep increase. This may first be ascribed to the fact that new fuel which has not been irradiated contains a fairly high content of moisture and gas molecules trapped between the dust particles as a result of the manufacturing process. When the TRISO fuel is heated, these components are evaporated and degassed, respectively, resulting in a significant amount internal pressure being exerted on the inner layer of the IPyC and SiC, leading to the expansion of TRISO coated particle. The second reason for this rapid change in the early days of irradiation in the irradiation process is because it is easier to cause radiation damage in fresh fuel which has not been irradiated, creating voids and bubbles than it is to fuel which has already been irradiated and thus has experienced radiation hardening. The reason for the second rapid increase is because the voids and bubbles which were formed as a result of radiation damage in the early days of irradiation they coalesce to form bigger entities (i.e. size growth) and also their

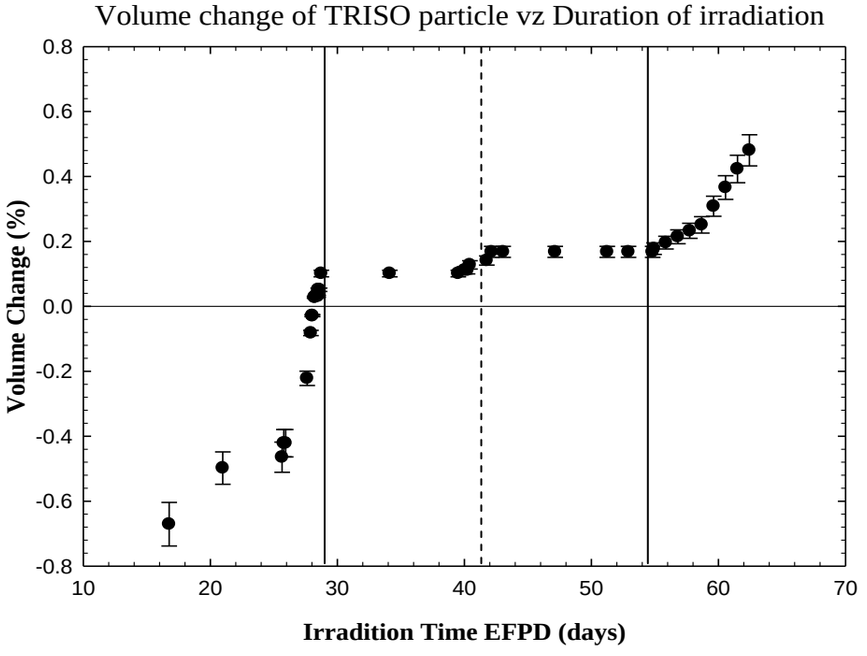

Figure 3.5: Volume change of TRISO coated particle as function of irradiation time (present study).

increase in number per unit volume (i.e. increase in density of voids/bubbles) combined with the fact that there is change in crystal structure caused by Frenkel pairs, results in the second phase of swelling [27, 42, 44, 47, 49, 51].

As discussed, Fig. 3.5 indicates volume change as a function of duration of irradiation resulting from the excess pressure in the cavities of the SiC. It may be divided into two sections: the section below 0% volume change and the section above this. Considering the section above 0% volume change and applying the classical drop model proposed by Wiedersich [58], noting that this part of the graph is positive and increasing, which means that the gas pressure P_g within the cavity is greater than the surface tension, γ, on the outside resulting in the cavity behaving like a gas bubble. The excess cavity pressure increases because of an insufficient number of available vacancies in the matrix required for equilibration. If sufficient vacancies are made available, e.g. by creep, dislocation and bubble

growth, it will continue to grow until the excess pressure equals zero. Continued bubble growth also requires diffusion of gas atoms as well as vacancies to the bubble. Bubble growth is also limited due to irradiation-induced gas atom re-solution from bubbles. For this reason this part of the graph is positive and increasing throughout the irradiation time period. It also shows that swelling due to bubble growth is linear.

On the lower part of Fig 3.5, below 0% volume change, the excess pressure is negative. In this case, the surface tension is greater than the internal gas pressure. There is a super-saturation of vacancies in the lattice and the cavities grow by the influx of cavities. Continued cavity growth under these conditions requires only excess vacancies in the lattice. For this reason this part of the graph is negative, showing shrinkage as result exposure to neutron flux [58, 60].

The other important finding is that the fuel can contract to a much higher absolute value than it can expand to, where from Fig. 3.5 it should be noted that fuel can expand to a maximum of about 0.50% and contract to about 0.70% of its original value.

Because the α-SiC has more vacancies than the β-SiC, it may be inferred from the above analysis that swelling in α-SiC is unstable because of the oversupply of vacancies and β-SiC swelling is much better behaved and stable because there are fewer vacancies [60, 61, 62].

3.2.3 Correlation between change in neutron flux and volume change

The effect of flux in volume change suggests that there are two competing forces playing a role i.e. surface tension and internal pressure in cavities, as observed in the correlation of irradiation time and volume change. However, in this case the crystal structure may also come into play. Volume change as a function of neutron

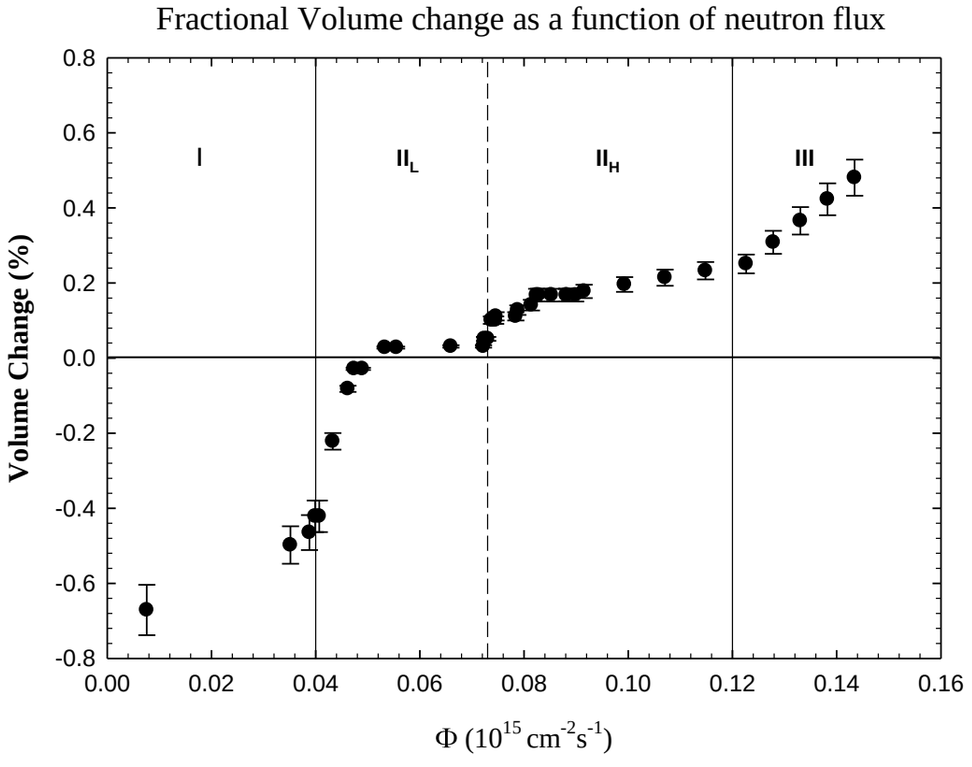

Figure 3.6: Volume change as function of flux (present study)

flux, Fig. 3.6, increases steadily from − 0.7% up to about −0.5%, where volume remains constant and then rises again, this time at a much lower rate until it reaches the peak at 0.5%. Figure 3.6 can be divided into three regions, namely:

REGION I: From a neutron flux of 0 to 0.040x10^{15} cm^{-2} s^{-1} is a pure α-SiC region. The concentration of α-SiC crystal structure dominates over any other crystal structure. Hence, the physical properties, e.g. the coefficient for thermal expansion, in this region will be those of α-SiC. Thus, volume expansion is driven by surface tension which is greater than the internal gas pressure. There is, therefore, super-saturation of vacancies in the lattice and expansion is as a result of growth of vacancies because of the influx of cavities.

REGION II: From a neutron flux of 0.040x10^{15} to 0.120x10^{15} cm^{-2}s^{-1} is a transition phase from α-SiC to β-SiC crystal structure which may be divided into

two sub-regions *viz:*

- **REGION[4] II_L: From $0.040x10^{15}$ to $0.070x10^{15}$ $cm^{-2}s^{-1}$:** This is a transition phase with high concentration in α-SiC and very little β-SiC. The physical properties of this structure are predominantly those of α–SiC. Although the concentration of β-SiC is very little in this phase, it is nevertheless present in sufficient quantity to distinguish its properties from those of pure α–SiC which occurs below $0.040x10^{15}$ cm^{-2} s^{-1}.

- **REGION[5] II_H: From $0.070x10^{15}$ $cm^{-2}s^{-1}$ to $0.120x10^{15}$ $cm^{-2}s^{-1}$:** This region of the transition phase has a very high concentration of β-SiC, its physical properties will predominantly be those of β-SiC, likewise α-SiC will only be present in sufficient quantities to distinguish it from pure β-SiC.

REGION III: From a neutron flux of $0.120x10^{15}$ $cm^{-2}s^{-1}$ to $0.140x10^{15}$ $cm^{-2}s^{-1}$ is the β-SiC region. The concentration of β-SiC crystal structure is much higher that the concentration of any other crystal structure. Hence, the physical properties of the material in this region are largely those of the β-SiC. Thus, the coefficient for thermal expansion will largely be that of β-SiC.

3.2.3.1 Comparison with results of other investigations

Volumetric expansion of the TRISO coated fuel particle has attracted a lot of interest in reactor fuel design because of its importance in safety aspects of the entire technology. As a result of this a number investigations have been conducted to determine how the neutron flux to which it is exposed will affect its dimensional change. The results of some of the investigations which have been conducted are described below.

[4] L refers to the lower end of the transition state
[5] H refers to the higher end of the transition state

3.2.3.1.1 Research conducted under the International Nuclear Energy Research Initiative (INERI)

A number of studies have been conducted in this regard and all confirm the findings obtained by the present study that there is relationship between volume change of TRISO coated particle and the neutron dose to which it is exposed as indicated in Fig. 3.7, which for ease of comparison has been placed on the same page with Fig. 3.8 at the end of this section. One such study was that conducted under international nuclear energy research initiative (INERI) made up of Idaho National Engineering and Environmental Laboratory (INEEL), Massachusetts Institute of Technology (MIT) and the French Centre d'Etude Atomiques (CEA) [22]. When % volume change is plotted against neutron fluence instead of against the flux, Fig 3.7 is obtained which is in good agreement with that obtained by Price [22] in the temperature range of 600°C-1000°C as indicated in Fig. 3.8.

The main reason why the % volume change *versus* fluence obtained in this investigation is different from that obtained by Price, is because the study by Price was specifically based on β-SiC only whereas in this study the experimental sample was made up of both α-SiC and β-SiC allotropes, each of which has its own physical properties e.g. volumetric expansion coefficients, and when blended together in a mixture as is the case in SiC of the present study, they will present the coefficient for thermal expansion which is completely different from either of the two. It is, therefore, very important that when a comparative study of performance of a number of fuel elements is conducted, an effort should be made to understand the compositions and the irradiation history of samples with which the test sample is being compared to. Such experimental errors could potentially cost the organisation significant amount of financial resources if they went unnoticed. Performance in this context refers to the ability of TRISO coated particle to retain the fission products within the protective layers of the TRISO coated particle.

It should also be noted that Fig. 3.6 is different from Fig. 3.7. The explanation lies in the dimensional analysis of units of flux and fluence.

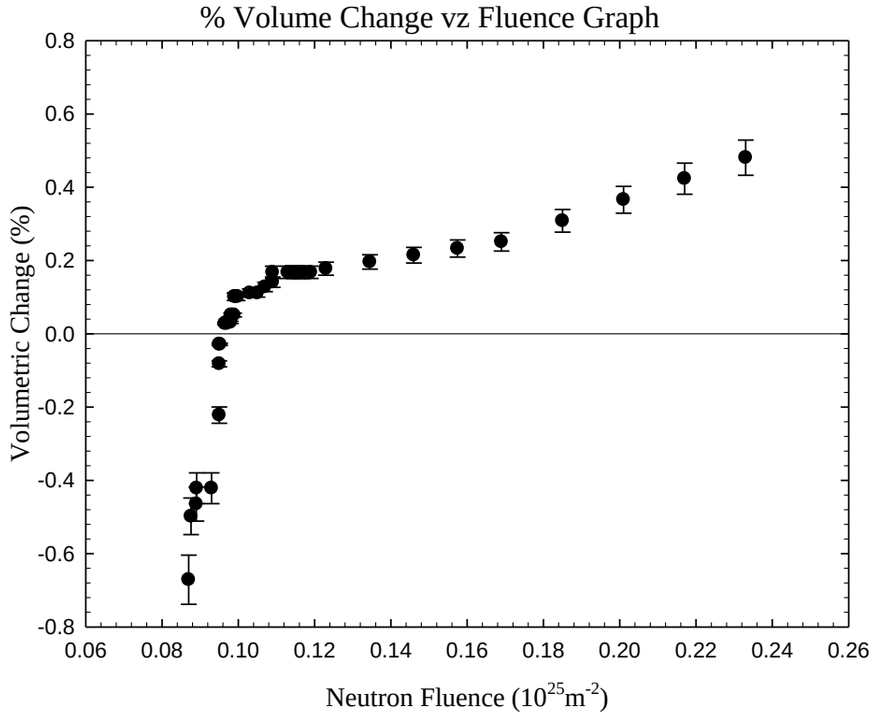

Figure 3.7: The effect of fluence on the change in volume of TRISO coated particle [Present study].

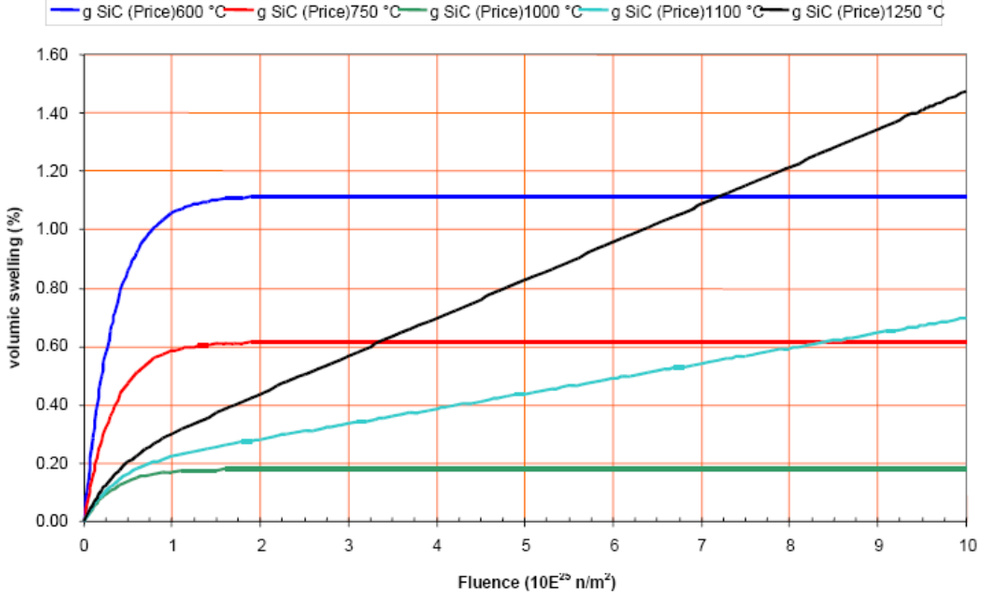

Figure 3.8: Swelling of β-SiC Pyrocarbon as a function of neutron fluence (taken from Figure 1-22 of [22]).

Flux is a derived unit consisting of per length squared per unit time ($L^{-2}T^{-1}$) which is often $cm^{-2}s^{-1}$ or m^{-2} s^{-1} where as fluence is a basic unit of L^{-2} and as already stated above it may either be cm^{-2} or m^{-2}. Hence, Fig. 3.6 i.e. the graph of % volume change *versus* flux is a compound graph obtained by dividing the % volume change *versus* fluence i.e. Fig. 3.7 by the graph of % volume change *versus* duration of irradiation Fig. 3.5. That is the reason why this graph i.e. Fig. 3.6 has the features of both Fig. 3.5 and Fig. 3.7.

3.2.3.1.2 Investigation by Argonne National Laboratory (US) and Bochvar Institute (Russia)

In the study conducted by Rest *et al*. [59], a 10% enriched uranium fuel was used to investigate key irradiation-induced swelling mechanisms. The focus of the study was to illustrate the difference between gas-driven growth and bias-driven (void) growth of a cavity and has established that the void growth mechanism results in significantly more swelling than the bubble driven swelling. This is because, under steady state conditions, the number of vacancies will be equal to the number of interstitials and the rate of combination between vacancies and interstitials will be steady, in which case the volume of a cavity will remain constant. However, if the conditions are such that there is a decrease in vacancy concentration, this will cause a decrease in the recombination of vacancies and interstitials and result in a higher concentration of interstitials which will lead to an increase in nucleation and growth of cavity and a higher values of dislocation density.

Instead of looking at the swelling of the entire fuel, the study by Rest *et al*.[59] focuses on the microscopic scale in which a correlation is drawn between the swelling of a cavity and the excess cavity pressure given by $P_g - 2\gamma/r - \sigma$. When the excess cavity pressure is plotted against the irradiation time, Fig. 3.9 is obtained which is in agreement with Fig. 3.5 of this study.

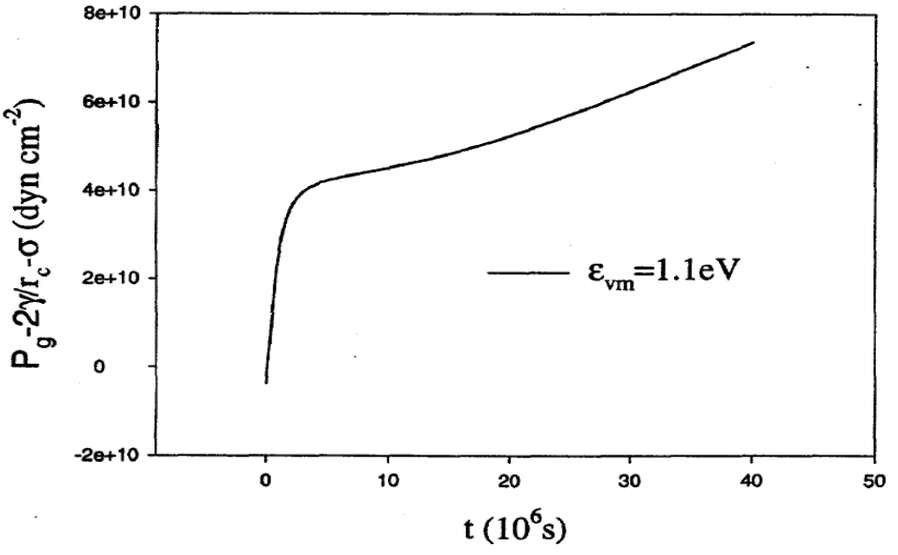

Figure 3.9: Excess internal pressure as function of irradiation time (taken from [59]).

This is expected since Rest *et al*. [59] measured *the cause of an effect* i.e. excess internal pressure, whereas in this study *the effect of the cause* (change in volume) is measured and the results are in good agreement since both are plotted against time, where the variables indicated on the graph refer to

- P_g is the gas pressure within the cavity,
- $2\gamma/r$ is the surface tension,
- σ is the stress to which the cavity is subjected to and
- ε_{vm} is the vacancy migration energy.

It is evident that the two competing forces i.e. surface tension and partial pressure are important variables in as far as dimensional change of the TRISO coated particle is concerned, since the particle will contract or expand depending on which is greater.

3.2.4 Correlation between increase in irradiation temperature and volume change

In addition to introducing all other effects referred to in Section 3.2.2 earlier, the most important effect is change in crystal structure. According to Krishna [29] a single crystal of α-SiC can easily be transformed to β-SiC on annealing in argon at temperatures above 1673 K. This is particularly important information as it confirms the studies conducted by Oliviero and Was [33, 54, 61] in which helium was cited as being problematic in nuclear reactors.

Figure 3.10 is a graphical representation of the relationship between % volume change and irradiation temperature. This indicates the same correlations as were found between volume change and flux. However, it is observed that the slope of line **CD** is much steeper than that of line **AB**. The difference in steepness is an indication of the difference in the rates of expansion and contraction.

The explanation for this difference lies in the understanding of the crystal structure of the two materials; **CD** has a very high concentration of β-SiC while **AB** has a high concentration of α-SiC. The difference in concentration of cavities and interstitials in the two regions explains why there is difference in release rates and consequently in the steepness of the two lines. Based on this it can be inferred that when the TRISO coated particles are subjected to high temperature, not only will they expand and contract, they expand much quicker than they contract.

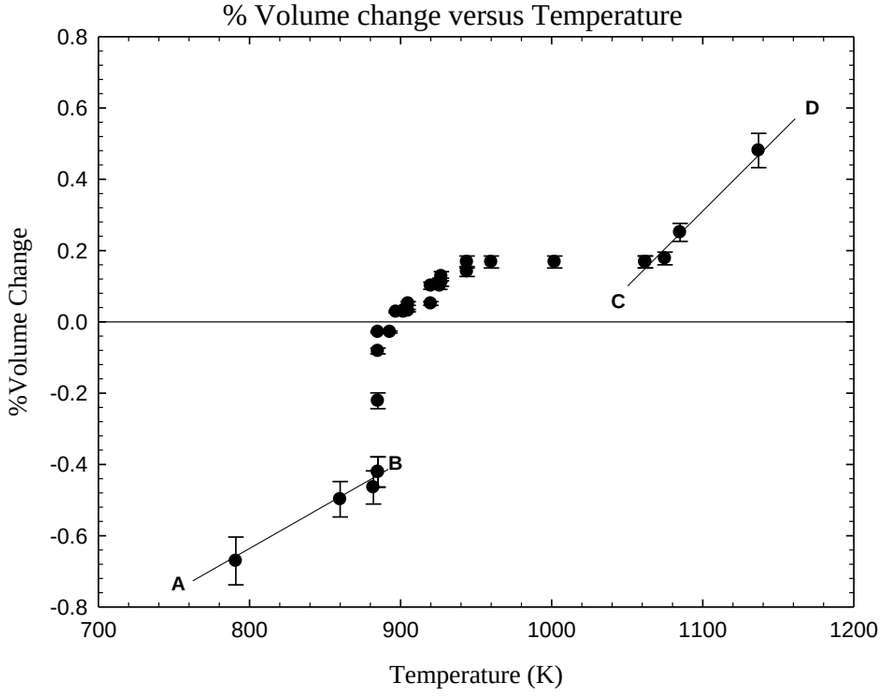

Figure.3.10: Effect of irradiation temperature on %volume change (present study).

3.2.5 Correlation between irradiation temperature and the diffusion coefficients of fission products

The diffusion of fission product from the HFR-K5 was modelled using the reduced Booth model (discussed in Section 2.6), because of its accuracy [21, 22, 39, 50, 53]. The diffusion coefficient *D* is calculated from the second part of equation (2.37) and that value takes the place of *D* in the first part of (2.37) to obtain R/B. All input data for calculating *D* are found in Table 2.2 This is an important input towards SOURCE TERM analysis as well as in accident analysis [37]. Beyond that, it serves as a good indicator of what fraction of actinides, noble gasses and particulates will constitute the SOURCE TERM. These ratios are of paramount importance in Probabilistic Risk Assessment (PRA) of public and worker dose as well as determining the extent of the emergency planning required [7, 64].

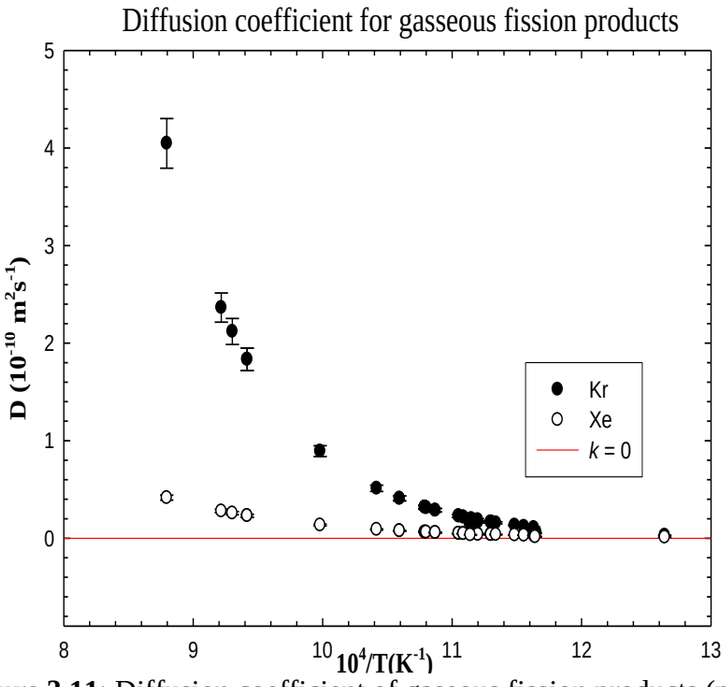

Figure 3.11: Diffusion coefficient of gaseous fission products (present study).

A plot of the diffusion coefficient of Krypton and Xenon illustrated in Fig. 3.11 clearly indicates that Krypton has a much higher diffusion rate than Xenon has, which is in agreement with the outcome of the study conducted by Prussin *et al.* [52] and that by Petti *et al.* [21, 50]. The determining factor on the diffusion rate of fission products is whether they are substitutional or interstitial atoms. The rate of the substitutional diffusion mechanism depends on the availability of the vacancy in the neighbouring lattice site; if there is no vacancy, there will be no atomic movement. The interstitial diffusion mechanism on the other hand does not depend on the availability of vacancies, the atoms can move at anytime regardless of whether there are vacancies or not. Thus, atoms diffusing by interstitial diffusion mechanism tend to diffuse much quicker than those diffusing by substitution mechanism.

3.2.6 Gaseous fission product release phenomena

There are a number of fission product models used all based on the Booth model [50]. The Release to Birth rate (R/B) of the HFR was calculated using the Booth

model for single and polycrystalline release through UO_2 and the results are described in the following sections.

3.2.6.1 Effect of variation of neutron flux on fission product release

The neutron flux plays a significant role in the release of fission products, primarily because of the radiation damage it incurs to the fuel specimen. It is, therefore, not surprising that there is a link between the release rate and the variation in neutron flux as indicated in Fig. 3.12 (For ease of comparison Figs. 3.12, 3.13 and 3.14 are grouped together at the end of this section).

Figure 3.12 shows the same qualitative features as was observed in Fig 3.6, in which the Φ-axis of both graphs is divided into a number of regions depending on the crystal structure of that region. Comparing this with the phase diagram depicted in Fig. 2.8, *one can draw the inference that region II in Figs. 3.6 and 3.12 are equivalent to the 50% dividing line in Fig. 2.8.*

From this, an inference can be drawn that the SOURCE TERM will increase as the neutron flux increases. Hence, it is predicted that by increasing the burnup and temperature of PBMR without changing the fuel design leads to a much higher SOURCE TERM. It is also worth noting that since the same nuclide tends to diffuse at different rates in the two phases i.e. in α-SiC and *β*-SiC, it can be deduced that everything being the same, the SOURCE TERM emanating from an α-SiC-based fuel will be different from that originating from a *β*-SiC-based fuel. The graphs indicate a number of factors that are important in fuel analysis and the figure may be divided into regions I, II and III. In the case of the variation of neutron flux on fission product release the corresponding regions are:

REGION I: This region extends from a neutron flux of about 0.01×10^{15} n $cm^{-2} \cdot s^{-1}$ to about 0.034×10^{15} n $cm^{-2} s^{-1}$, where there is a gradual increase in release rates correlating to the increase in neutron flux. This may be explained by noting that *α*-SiC is a dominant crystal structure in this region

which has a diffusion mechanism that is largely substitutional. Since, when there is no vacancy, there will be no atom movement to the next lattice, diffusion in this region takes place at a very slow rate than would have been the case had it been the interstitial mechanism.

REGION II: This extends from a neutron flux of $0.034x10^{15}$ n $cm^{-2}s^{-1}$to about $0.094x10^{15}$ n $cm^{-2}s^{-1}$, where the crystal structure is neither pure α-SiC nor pure β-SiC but a mixture of both. Hence, the diffusion mechanism is neither pure vacancy nor pure interstitial, but a mixture of the two. The gradient of the graph from $0.034x10^{15}$ n $cm^{-2}s^{-1}$ up to $0.075x10^{15}$ n $cm^{-2}s^{-1}$ is flatter than that of Region I just before it, indicating that there is a decrease in release rate. This corresponds to the beginning of the transition phase; the vacancy concentration which was high for the pure α-SiC has decreased as result of transition process, resulting in the decrease of diffusion by the substitution diffusion mechanism and a gradual increase by interstitial diffusion mechanism. The sub-region from $0.075x10^{15}$ n $cm^{-2.}s^{-1}$ to $0.094x10^{15}$ n $cm^{-2.}s^{-1}$ represents the late transition phase, which is dominated by β-SiC and the interstitial diffusion mechanism. As such, there will be an increase in the diffusion of interstitial atoms such as Ag and other metallic products.

REGION III: This extends from a neutron flux of $0.094x10^{15}$ $ncm^{-2}s^{-1}$ to $0.145x10^{15}$ n $cm^{-2}s^{-1}$, where the rel**e**ase is much higher than in the region that just before it, mainly because diffusion in the β-SiC is driven by the interstitial diffusion mechanism which is faster than the substitutional diffusion mechanism. Based on the level of Ag in the source-term, its atomic size relative to that of carbon and silicon in the SiC, and the diffusion mechanism of this region, it may be inferred that this is the region responsible for largest fraction of Ag release.

Looking at Fig. 3.12 along the Φ-axis, it is noticed that it can be divided into four different groups according to the lengths of half-lives ($t_{1/2}$) of nuclides in that

group. Beginning at the bottom of the release rates the following groups are observed:

GROUP I (Seconds Group): This group consists of all those nuclides which have $t_{1/2}$ in the range of seconds. Its members consist of ^{139}Xe and ^{90}Kr which have $t_{1/2}$ of 39.7 s and 32.3 s respectively.

GROUP II (Minutes Group): This consist of all those nuclides whose $t_{1/2}$ is in the order of minutes, and it consists of ^{89}Kr, ^{137}Xe, ^{138}Xe, ^{135m}Xe whose $t_{1/2}$ are 3.16 min, 3.84 min, 14.1 min and 15.3 min respectively.

GROUP III (Hours Group): This group consists of all those nuclides which have their $t_{1/2}$ in the range of hours. Its members are ^{87}Kr, ^{88}Kr, ^{85m}Kr and ^{135}Xe and have $t_{1/2}$ of 76 min (1.25 hrs), 2.48 hrs, 4.48 hrs and 9.1 hrs, respectively.

GROUP IV (Days Group): This consists of all those nuclides whose $t_{1/2}$ are in the order of days, and consist of ^{133}Xe and ^{131m}Xe with $t_{1/2}$ of 5.25 and 11.92 days, respectively.

A closer look indicates that the transition phase acts as filter, filtering fission products on the basis of their half life; the longer the half-life of a nuclide, the higher is the release rate. It is noted that it also acts as an inverter, inverting the release rate based on the relative atomic mass, A_r, as the crystal structure changes from α-SiC to β-SiC:

On the β-SiC side: within the same group, (e.g. hours group), *the larger the A_r value, the slower is the release rate.* For example, ^{87}Kr with the A_r value of 87 has a higher release rate than ^{135}Xe with the A_r value of 135, thus indicating that within the same group in the β-SiC structure, higher release rates are favoured by lower atomic mass numbers and that the atomic mass factor plays a much more significant role than the half-life factor.

On the α-SiC side: as shown in Fig 3.12, the release rates follows the opposite trend from that of β-SiC, implying that within the same group, *the larger A_r value, the higher is the release rate.*

3.2.6.2 Effect of changes in irradiation temperature on fission product release rate

The temperature affects fission product release in much the same way as neutron flux does, however it has fewer discontinuities than neutron flux as shown in Fig. 3.13. This is because as stated in Section 3.2.3.1.1, flux is a derived unit while temperature is a basic unit. Thus the nature of the graph of flux is influenced by that of other graphs out of which it is made, while it is not the case with temperature. Thus, as shown in Fig 3.13, the release *versus* temperature graph is smooth, increasing with the increase in temperature, which as indicated earlier, confirms that there is tendency towards higher fission product release rate as the crystal structure changes from α-SiC to β-SiC.

Again, as pointed out in Section 3.2.6.1, the role of the relative atomic mass and the half lives of nuclides in the diffusion have a similar effect on fission product release although with fewer discontinuities than between the transitions of various crystal structures.

It is imperative that whenever the *R/B* graphs are interpreted, they should be studied in conjunction with Fig. 2.8 since it provides the basis of physical properties of each of the crystal structures noticed in SiC and the explanation for the behaviour of fission products in each one of them.

3.2.6.3 Effect of duration of irradiation on the release of fission product

The correlation between the duration of irradiation and fission product release rates is illustrated by Fig. 3.14. The graph indicates that there is large 'burst' of

release in the first two months of irradiation. This is because the large amounts of air and moisture introduced in the fuel during the manufacturing phase are trapped between voids and vacancies which could not be removed by other means. As the number of days passes by, holding it at the same temperature, the release levels out since most of the free air and moisture has been degassed or evaporated respectively at the beginning of the irradiation period. This is the reason why the slope of the graph in Region III is less steep than the slope in Region I.

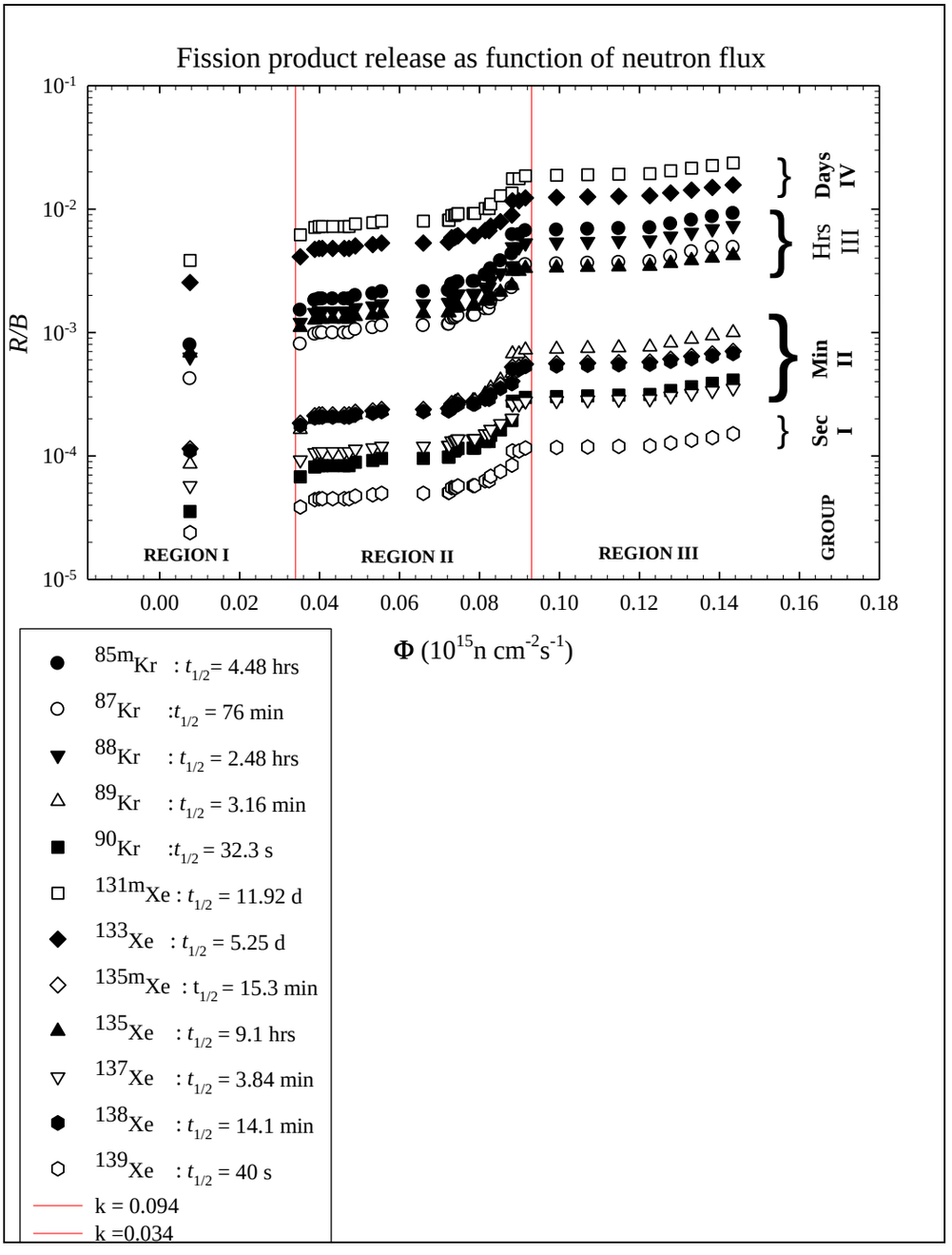

Figure 3.12: Fission product release as function of neutron flux (Present Study).

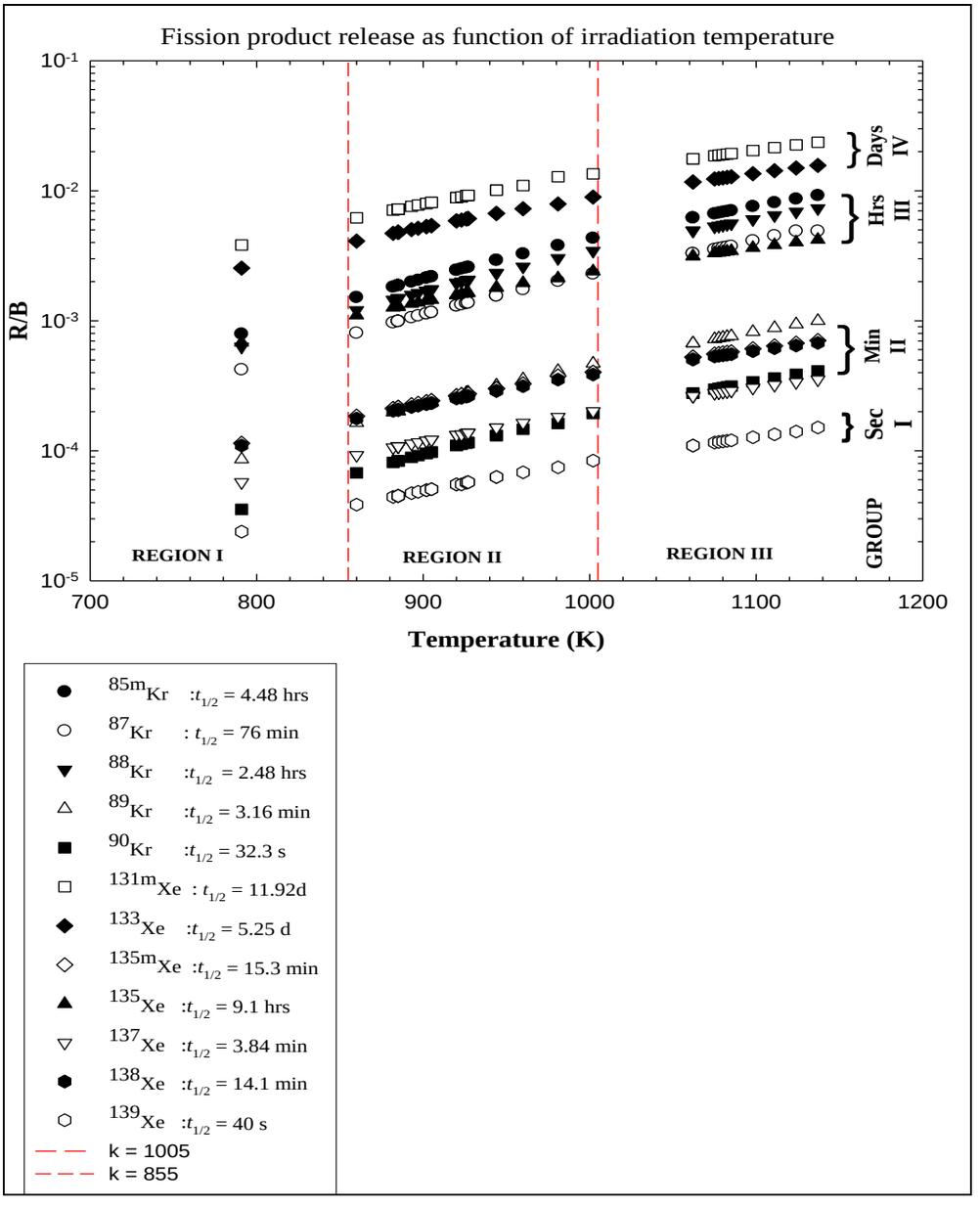

Figure 3.13: Fission product release as function of irradiation temperature (present study).

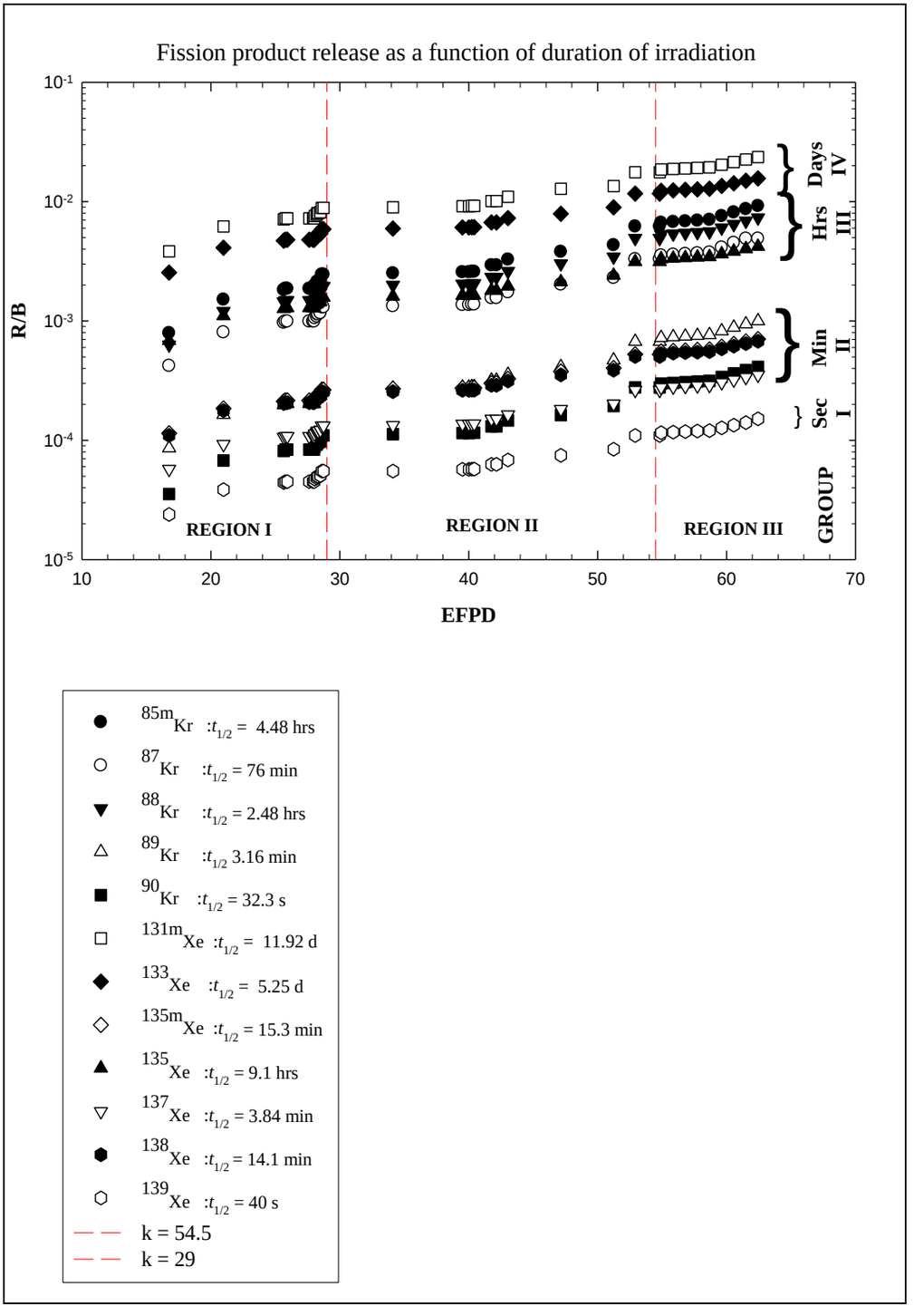

Figure 3.14: Fission product release as function of duration of irradiation (present study).

CHAPTER 4

Research Findings

The investigation has uncovered a number of important findings which are important from the fuel design perspective in that if not prevented or managed properly can lead to failure of SiC to effectively perform its function as a barrier to fission product migration which will subsequently lead to failure of the entire fuel sphere. To this end, a number of intervention measures recommended in Chapter 5 will be needed to prevent the SiC and other layers from failing. If this is not done, the present problems of high SOURCE TERM release that PBMR is experiencing will not be resolved. The sections below summarise the present research findings.

4.1 Irradiation of TRISO coated particle results in crystal structure transformation of the SiC

The results indicate that silicon carbide undergoes severe crystal transformation when subjected to high neutron flux and high temperatures. This is a particularly important consideration because fission products diffuse at different rates in different crystal structures depending on whether it is α-SiC or β-SiC. Because of this, the SOURCE TERM will be comprised of different nuclides at different activity levels, for example, at low neutron flux and temperature there will be less Ag. As the temperature and flux increases, the levels of long-lived nuclides (i.e. nuclides with $t_{1/2}$ in order of days and longer as discussed in Section 3.2.6.1 and indicated in Figs. 3.12, 3.13 and 3.14) in the SOURCE TERM will also increase. The nuclides that are expected to dominate the sources term based on their long half lives are:

- fission products: ^{85}Kr, ^{90}Sr, ^{125}Sb, ^{106}Ru, ^{137}Cs, ^{131m}Xe, ^{133}Xe, ^{134}Cs, ^{131}I, ^{110m}Ag,
- activation products: ^{60}Co, ^{55}Fe, ^{63}Ni

- water and impurity activation products: ^{3}H, ^{14}C.

It is important to bear this in mind as they will continue to be of concern as long as the present fuel design is used. Furthermore, analysis indicates that as the temperature increases, there is a tendency for crystal structure to change towards the higher packing factor. Hence, a plot of the release rate *versus* the packing factor suggests higher release rates as the packing factor increase**.**

4.2 Long-lived fission products tend to dominate the release fractions

The analysis indicates that the transition crystal-structure acts as a filter, filtering the release rates based on their half-lives. Based on this, it has been observed that the longer the half-life of a nuclide, the higher is the release rate of that nuclide in comparison with other isotopes of the same element. This is confirmed by the four half-life groups referred to earlier (see Section 3.2.6.1). However, in cases where there are two nuclides with the same half-life but different atomic masses, the atomic mass factor will come into effect, inverting release rates on the basis of the magnitude of the atomic masses; on the β-SiC side, within the same group, the larger the atomic mass, the smaller the release rate. This is the reason why ^{87}Kr has a higher release rate than that of ^{135}Xe. On the α-SiC side the order is reversed; the release rate of ^{87}Kr is lower than that of ^{135}Xe.

The above observations indicate that the selection of the composition of SiC and the level of purity play a significant role in the level of nuclides release: as seen in Fig. 3.12 (REGION I), the higher the purity of α-SiC, the lower is the release rate. However, the disadvantage of using fuel rich in α-SiC as shown in Fig. 2.8 and Fig. 3.12 is that the operating temperature is limited to a maximum of 1415°C. On the other hand, using fuel rich in β-SiC has an advantage that the reactor can reach very high temperatures, as high as 2830°C before it melts. The disadvantage is that as the temperature increases, there is a corresponding increase in release rates (see REGION III in Fig. 3.12) reaching release levels that are much higher than are observed in α-SiC. Fuel design needs to take these factors into considerations when determining the reactor operating temperature. Another important aspect

that must also be borne in mind is that these nuclides i.e. fission products and activation products all decay by emitting β's and γ's [65] which will present a huge maintenance problem if ignored in the design phase of this project.

4.3 SiC is very susceptible to corrosion by metallic fission products and carbon monoxide

As stated in Section 2.3.1, the present investigation indicates that SiC is very susceptible to corrosion by metallic fission product as well as by carbon monoxide. This is of prime importance in the selection of fuel cladding material since alternate cladding material like ZrC has a much better resistance to corrosion. High levels of carbon monoxide are even worse since it has two detrimental effects *viz.* chemically corroding the SiC as well as increasing the internal pressure, thus increasing the probability of a Pressure Vessel Failure accident of the TRISO-coated particle.

The present analysis indicates that SiC layers are attacked locally, and that although palladium is of prime concern, there are other metallic products like Ag, Ru and Rh which have also been identified as contributing to the corrosion of the coated particle. Silver in high concentration will attack SiC, displaying Arrhenius behaviour with about the same activation energy as Pd. At low concentration, typically of operational fuel particles, silver can escape from the particles, diffusing through the intact SiC. In addition, palladium and carbon monoxide have been found to have higher concentration on the colder side than on the hotter side of the TRISO coated particle, thus, indicating that a temperature gradient on the fuel is undesirable in as far as fuel failure analysis is concerned. It is, therefore, imperative that this matter is taken into consideration in the design of fuel loading device and the reactor core to ensure that the fuel spheres are in a constant rotational movement all the time to prevent one side being exposed to higher temperature than the other.

With regard to the time dependence of SiC corrosion, there was an unquestionable time dependence of palladium interaction with SiC, yet the same could not be said

for rare-earth carbides. On the question of Ag, no time-temperature dependence of silver interaction with SiC could be determined.

Palladium attack of SiC is the main reason why the silicon carbide loses its effectiveness as fission-product barrier prematurely and hence the high fission product release rates in the SOURCE TERM, and needs to be prevented.

4.4 High internal pressure will lead to catastrophic failure of the SiC Pressure Vessel

As discussed in Section 2.3.4, gaseous fission products like Xe, Kr, I together with carbon monoxide and carbon dioxide exert a tremendous amount of pressure on the inner layers of the coated particle which if not maintained below their respective breaking strengths will lead to catastrophic failure of the pressure vessel of the TRISO coated particle and thus result in high fission-product release rates. High production rates of oxygen exacerbates the situation even further since it increases the partial pressure of CO, which is undesirable in the fuel because of its dual detrimental effect referred to earlier. Thus, the level of carbon monoxide must be kept to a minimum if the lifespan of the coated particle is to be preserved.

4.5 There is a link between the amounts of inert gas in the TRISO coated particle and the dimensional change it experiences

Inert gasses such as Helium, Krypton and Xenon are undesirable in the coated particle as they are responsible for the high concentration of voids and bubbles that are often seen in the fuel. They act as nucleation sites which are critical for the nucleation process through which voids and bubbles are formed, which eventually through the coalescence process grow in size and result in swelling of the fuel.

Having identified the findings of this project in this chapter, it is now left to the next chapter i.e. Chapter 5 to develop and consolidate recommendations of how

they will be addressed to prevent them from occurring. One of the most critical findings that will be addressed is recommending the best operating conditions for the PBMR that ensure that the TRISO coated particle maintains its integrity for the entire duration of the operating cycle of the PBMR.

CHAPTER 5

Conclusions and Recommendations

The recommendations made here are based on the findings of this investigation as well as from those of other researchers in the field of fuel technology. They will address two important aspects of the fuel, first to identify safe operating conditions of the present fuel design if it becomes the final fuel design for the PBMR seeing that there are a number of alternate fuels being developed with much better resistance to metallic and chemical attack. This is summarised under Section 5.1 of this Research Report and is aimed at minimising fission product release rate and subsequent reduction of the SOURCE TERM. The second aspect concerns recommendations described in Sections 5.2 to 5.4 to identify suitable alternative designs with better resistance to chemical corrosion and metallic attack if no solution is found to the present high SOURCE TERM problem.

5.1 Limiting operating conditions for the present fuel design

In order to prevent excessive release of fission products it is critically important to acknowledge the limitations imposed by the chemical as well physical properties of the TRISO coated particle and make every effort to avoid operating the reactor outside these boundaries. To achieve this, it is recommended that fuel is never subjected to any temperature higher than the top boundary of the α-SiC region as shown in Fig. 2.8, i.e. 1415°C which is the upper most limit which must never be exceeded. A more detailed analysis of this is provided in the following sections.

5.1.1 Limitations imposed by the chemical composition of SiC

Since the release rate of fission product is related to the amount of α-SiC and β-SiC in the fuel with higher release rates being associated with larger β-SiC region,

it is recommended that the amount of β-SiC in the entire SiC is kept as low as reasonably achievable. Furthermore, since this area is dependent on the carbon concentration, it is recommended that the concentration of carbon in the SiC must never be less than 50%. Below this level the β-SiC becomes the dominant component resulting in higher release rates of fission products as a result of change in crystal structure and subsequent change in the concentration of vacancies.

5.1.2 Upper temperature limit

As indicated in Fig. 2.8 and Fig. 3.13 above the α-SiC region is characterised by a much lower release rates than the β-SiC region, thus the ideal reactor operating region is the former rather than the latter. Since the upper temperature limit (T_{limit}) of the α-SiC region is 1415°C, it is recommended that the fuel temperature never exceeds the top limit of 1415°C. Beyond this temperature the SiC begins to melt and the TRISO particle loses its geometry and reactor enters accident operating conditions. In order to prevent the fuel from ever exceeding the 1415°C upper limit, an upper operating temperature limit of 1000°C is recommended. This will provide the reactor operators with a temperature margin of 415°C which translates to sufficient time in which to react if an unusual event were to occur which may result in an increase in temperature.

5.1.3 Aspects of PBMR Safety

It can be seen that sections 5.1.1 and 5.1.2 deal with two distinctively different aspects of reactor safety: *prevention of fission product release from intact fuel* (where no fuel failure has occurred) (Section 5.1.1) and *prevention of temperature-induced fuel failure* (Section 5.1.2). These paragraphs may be summarised as follows:

- To minimise fission product release from intact fuel, the concentration of carbon in the entire SiC must be ≥ 50%. This will ensure that the area of α-SiC region is much bigger than that of β-SiC, and thus result in lower fission product release rates.

- To reduce the probability of premature temperature-induced failure, T_{limit} must be less than 1415°C ($T_{limit} < 1415°C$).

5.1.4 Upper limit of the internal partial pressure.

As stated earlier, gasses in the TRISO coated particle exert an enormous amount of pressure on its layers which if not controlled could lead to catastrofic failure of the coated particle. In order to prevent this, it is recommended that a two-pronged approach is developed that will cap the partial pressure of carbon monoxide in the TRISO coated particle since it has the highest partial pressure of all the gasses produced, and secondly, cap the total pressure resulting from all gasses, i.e fission products and CO. From this, it is recommended that:

- As long as the ratio of oxygen to uranium **(**O/U**)** in the fuel is less or equal to 2 (i.e. $O/U \leq 2$) (such as in the UO_2 fuel used in the PBMR), the partial pressure of carbon monoxide in the TRISO coated particle must never exceed the top limit of 100 MPa. This will reduce the energy with which CO interacts with SiC and prevent failure.
- The top limit due to all gasses in the TRISO coated particle must never exceed 350 MPa for the same reason stated above. The two points are summarised mathematically by Eq. (2.25)**.**

5.2 Design fuels with better performance under irradiation conditions

Corrosion of SiC by palladium and carbon monoxides is a very serious problem for the PBMR which if not curbed could potentially affect its chances of competing with other nuclear reactor designs in the market. This is particularly important since the safety features of the reactor and public safety carry a significant weight in the selection criteria of new reactor design. It is, therefore, important that timely investment of resources is made towards the research and development (R&D) of fuel-design that will be resistant to attack of these materials. Without this being addressed the solution of the high SOURCE TERM

may not be resolved. Below are methods which could potentially be solutions to chemical attack.

5.2.1 Formulate fuels that can form oxides with rare-earth fission products readily

Movement of rare-earth fission products e.g. Pu, Ce and Eu in the TRISO coated particle tends to increase the chance of corrosion of the SiC by metallic fission products. This can be eliminated if the rare-earth fission products exist as oxides rather than in other forms. The stoichiometry of the fuel, particularly the kernel, must be controlled such that it produces rare-earth fission products that have a higher tendency to form oxides rather than any other compound. On a laboratory scale this has been proven to be a viable and very effective mechanism of preventing metallic attack and large scale production is being investigated in other countries [43].

5.2.2 Add the second SiC layer between the buffer layer and the kernel

Inclusion of an additional SiC layer between the kernel and the buffer layer can significantly improve the performance of the fuel by reducing the corrosive effects of palladium and carbon monoxide, thus extending the life-span of the TRISO fuel particle. This has been found to be a relatively cost-effective option in reducing corrosion of SiC by palladium and carbon monoxide.

5.2.3 Design a manufacturing process that will prevent formation of large grain boundaries

Extensive studies indicate that transport of metallic fission products such as palladium involves SiC grain boundaries that are large and columnar almost extensively. They provide a more direct diffusion path than small equiaxed grains do, as such large columnar grains with disordered boundaries are undesirable from the metallic retention point of view. In summary, the more faulted the SiC is, the greater the probability that it will act as a site for attack and therefore the greater

the risk of failure. Thus, voids or gaps are undesirable as far as SiC attack is concerned.

5.3 Include getter material in the fuel composition

Addition of getter material that will react with Pd before it attacks SiC will significantly reduce the chances of Pd-SiC interaction and prolong the life-span of the fuel [66, 67]. This was observed in the studies conducted by Minato [39] in which it was shown that the chemical reactions taking place in the kernel can be steered in such a way that they react preferentially with palladium, thus eliminating it from the system. This can be achieved by including an element or compound which has a high affinity for palladium in the composition that will react with it before it interacts with SiC and thus remove it from the system.

5.3.1 Inclusion of an additional (SiC+PyC) layer as oxygen getter

Applying additional layers of SiC and PyC has been proven to be very effective in the reduction of Pd attack. One such fuel composition that employs this concept is that of Minato *et al.* [39], in which an additional barrier added inside the SiC, made up of either (SiC + PyC) or (an additional SiC layer that contain free carbon) reacts with palladium thus reducing its concentration in the TRISO coated particle and thus preventing it from reaching the SiC layer. This reduces the chance of Pd-SiC interaction, and consequently results in the reduction of failure probability of the SiC. The second composition which employs a binary compound ZrC as an oxygen getter simply known as UO_2* is described in the following section.

5.3.2 Application of ZrC as an oxygen getter

The research conducted by Verfondern *et al.* [68] at the Research Center Jülich in Germany discovered that by inserting a thin layer of ZrC directly on the UO_2 kernel followed by the buffer layer, and then the rest of other layers as commonly used in SiC TRISO coated particle, tremendously improves the performance of

the fuel. This fuel, often designated UO_2*, is made up of 9-14 μm layer of ZrC and when tested against other SiC TRISO coated particle has been found to be the only one that released less than 0.01% fission products after being heated for 10 000 hours at temperatures of 1200, 1350 and 1500°C. It has also been found to have a much better retention of Cs, Ce ,^{110m}Ag and ^{155}Eu. This is a significant improvement since the release of ^{155}Eu and ^{110m}Ag isotopes from the SiC which had no ZrC layer were about 15% and 100%, respectively, when heated to 1500°C. Thus, addition of the ZrC layer over the UO_2 has led to tremendous improvement in the retention these isotopes i.e. (^{155}Eu and ^{110m}Ag isotopes) [68], particulaly ^{110m}Ag since it has been troubling fuel designers for quite some time.

In addition to improving the retention of fission products, it has been shown that ZrC also served to restrict the swelling of UO_2 to only 1% whereas the same kernels in regular TRISO particles expanded by 10.6% [68].

5.4 Replace SiC with ZrC

Zirconium carbide (ZrC) is one of the materials that is being investigated for use in fuel cladding of Generation IV reactors (Gen IV). It has been found to have a much higher melting point than SiC and also a much better resistance to metallic attack as well as a much higher retention of metallic fission products than SiC. It has also been shown that it has very low damage and moderate swelling under ion irradiation at room temperature [48].

In one of the Japanese experiments where both SiC and ZrC TRISO particles were irraditated side-by-side to a burnup of up to 4.5% FIMA at temperatures ranging from 1400°C to 1650°C, it has been shown that there was complete coating failure of only 1 particle out of 2400 particles of ZrC-based TRISO coated particle, whereas in the SiC-based particles there was complete coating failure of 20 out of 2400 particles [68], which shows that ZrC has much superior qualities than its SiC counter part.

Exposure of irradiated particles to higher temperatures revealed the same trend except that there were more SiC-based coated particles that failed than those that were ZrC-based. For example, when both irradiated particles were heated to 2400°C at the rate of 1°C s^{-1} and held at 2400°C for more than 1.5 hours, there was only 1% failure of particles based on ZrC whereas there was 90% failure on particles based on SiC in the same period. It has also be shown that the ZrC-based fuel particle retained Cs and Ag much better than the SiC-based particle. However, the release of ^{106}Ru was found to be much higher in ZrC-based samples than has been the case in the SiC.

In conclusion, for reasons stated above, ZrC is a much better alternative to fission product retention than SiC and its application to solve the PBMR SOURCE TERM problems should be investigated.

DEFINITIONS

Allotropy refers to the reversible phenomenon by which materials may exist in more than one structure.

Amorphisation refers to a transformation in crystal structure of a material from one polytype or allotrope to another

Amorphous: The property of material not having a crystal structure

Anisotropy: The property of material being directionally dependent, changes in a physical property (absorbance, refractive index, density, etc.) for some material when measured along different axes.

Atomic Packing Factor (APF): The fraction of volume in a crystal structure that is occupied by atoms.

Burn up: The amount of fuel used up in a nuclear reactor, measured in % FIMA

Debye Temperature: The temperature of a crystal's highest normal mode of vibration, i.e., the highest temperature that can be achieved due to a single normal vibration of a crystal.

Diffusion coefficient: A factor of proportionality representing the amount of substance in grams diffusing across an area 1 cm^2 through a unit concentration in 1s of time.

Fertile material: The material that will capture a neutron and undergo transmutation by radioactive decay into a fissile material, e.g. ^{238}U

Fissile nuclear material: The material that will undergo fission when bombarded by neutrons, e.g.^{235}U

Frenkel defect: Also called a Frenkel pair or Frenkel disorder is a compound crystallographic defect in which an interstitial lies near the vacancy. A Frenkel defect forms when an atom or ion leaves its place in the lattice (leaving a vacancy), and lodges nearby in the crystal (becoming an interstitial).

Gettering : The process of removing device-degrading impurities from the active regions of the material which have the properties to render it ineffective in carrying out its functions e.g. and Palladium and Oxygen in TRISO coated particle. The general mechanism by which gettering removes impurities from device regions may be described by the following steps: 1) The impurities to be

gettered are released into solid solution from whatever precipitate they are in; 2) They undergo diffusion through the silicon; 3) They are trapped by defects such as dislocations or precipitates in an area away from device regions.

Heavy Metal Loading: Fraction of heavy metal content in the fuel kernel and have heavy influence in the burnup of the fuel

Interstitial atom: is an atom that is located in a position of a crystal that is not a regular crystal site

Interstitial compounds: Compounds formed by reaction of at least two interstitial atoms and occupies the interstitial spaces of the crystal structure.

Metastable phases: refer to phases with a free energy higher than that of the stable phase under the prevailing conditions of temperature and pressure.

Polymorphism: The property of a material to exist in more than type of space lattice in the solid state.

Release-to-Birth rate (R/B): The rate at which fission products are produced from fission process and decay of parent nuclides to the rate at which they escape out of the fuel element

Self-diffusion: Spontaneous movement of an atom to a new site in a crystal of its own species

Source-Term: The amount of radioactive material released to the environment following a nuclear accident.

Vacancy type imperfection: A type of lattice imperfection in which an individual atom site is temporarily unoccupied. Diffusion is generally visualized as the shifting of vacancies.

ACRONYMS

ALARA: As Low As Reasonably Achievable

Asgisa: Accelerated and shared Growth Initiative for South Africa

AVR: Arbeitsgemeinschaft Versuchs Reaktor

BCC: Body Centred Cubic

BWR: Boiling Water Reactor

dpa: displacements per atom

DPP: Demonstration Power Plant

EFPD: Effective Full Power Days

EIA: Environmental Impact Assessment

EPZ: Emergency Planning Zone

FCC: Face Centred Cubic

FE: Fuel Element

FIMA: Fraction Initial heavy Metal Atoms Fissioned

FY: Fission Yield

HCP: Hexagonal Close Packed

HFR: High Flux material test Reactor

HPC: High Pressure Compressor

HTGR: High Temperature Gas-cooled Reactor

ILTI: Inner Low Temperature Isotropic layer

IPP: Independent Power Producers

IPyC: Inner Pyrocarbon

JMTR: Japan Material Test Reactor

KNPS: Koeberg Nuclear Power Station

LEU: Low Enrich Uranium

LPC: Low Pressure Compressor

LWR: Light Water Reactor

MW_{th}: Mega Watt thermal

NEMA: National Environmental Management Act

oLTI: Outer Low Temperature Isotropic layer

OPyC: Outer Pyrocarbon

PBMR: Pebble Bed Modular Reactor

PCU: Power Conversion Unit

PF: Packing Factor

PWR: Pressurised Water-cooled Reactor

RoD: Record of Decision.

RPV: Reactor Pressure Vessel

TRISO: Tri-isotropic

UTS: Ultimate Tensile Strength

ZrC: Zirconium Carbide

REFERENCES

1. Asgisa. *Accelerated and Shared Growth Initiative for South Africa (AsgiSA),* Parliament. [Online] 18 May 2007. [Cited: 18 02 2009.] http://www.info.gov.za/asgisa/asgisa.htm.

2. *Nuclear Energy Policy For The republic Of South Africa.* Pretoria: Department of Minerals and Energy, 2008.

3. http://www.pbmr.co.za/index.asp?Content=201. *Environmental Impact Report.* [Online] 05 09 2008. [Cited: 20 02 2009.]

4. *Regulation No R388;Regulations In terms of sections 36, read with section 47 of the NNR Act, 1999 On Safety Standards And Regulatory Practices.* Pretoria:DME, 2006.

5. Protocol, Kyoto**;** http://unfccc.int/resource/docs/convkp/kpeng.html. *http://unfccc.int/resource/docs/convkp/kpeng.html.* [Online] 2002. [Cited: 18 02 2009.]

6. D Swanepoel**;** *Appeal against the Record of Decision (RoD)granted to the Nuclear Energy Corporation Of South Africa (NECSA)for the Pilot Fuel Plant(PFP*. Pretoria: Cape High Court, 2007.

7. National Nuclear Regulator: *Emergency Preparedness And Response Requirements For Nuclear Installations, rev 0,* 2005. Centurion

8. JJ Van der Merwe; *Verification and Validation of the PBMR Models and codes used to predict Gaseous Fission Product Release From Spherical Fuel Element.* Johannesburg: Randse Afrikaanse Universiteit, 2004.

9. R Moormann**;** *A Safety re-evaluation of the AVR Pebble Bed Reactor operation and its consequences for future HTR concepts.* Washington: HTR2008, 2008.

10. J Slabber**;** *Lecture Notes: Physics and engineering for the PBMR-400 Demonstration Power Plant.* Pretoria: PBMR(Pty)Ltd, 2005.

11. YA Cengel and MA Bole**;** *Thermodynamics: An Engineering Approach.* Toronto: Mc Graw-Hill, 1998. ISBN 0-07-011927-9.

12. EE Lewis**;** *Fundamentals Of Nuclear Reactor Physics.* Amsterdam: Elsevier, 2008.

13. KS Krane**;** *Introductory Nuclear physics.* Singapore: John Wiley and Sons, 1988.

14. C Pringle**;**Revised EIA plan for Eskom nuclear project opens for comment onb monday. *Creamer's Media Engineering News.* 2009.

15. DME**;** *National Nuclear Regulator Act.* s.l.: Republic Of south Africa, 1999.

16. DME**;** *Nuclear Energy Act.* 46, Pretoria: Republic of South Africa, 1999, Vol. 414.

17. IAEA**;** *Site Evaluation for Nuclear Installations, Safety Requirements No NS-R-3.* Vienna: International Atomic Energy Agency, 2003.

18. http://txweb.eskom.co.za/users/nc_reports/. *http://txweb.eskom.co.za/users/nc_reports/.* [Online] Eskom, 18 02 2009. [Cited: 18 02 2009.]

19. Eskom,National Control Morning Report. *http://txweb.eskom.co.za/users/nc_reports/.* [Online] Eskom, 18 02 2009. [Cited: 18 02 2009.] http://txweb.eskom.co.za/users/nc_reports/.

20. WJ Kovacs, K Bongartz, and D Goodin**;** *TRISO-Coated HTGR Fuel Pressure Vessel Performance Models.* DOE: GA Technologies, 1983.

21. MA Futterer, H Lohner, R Conrad, S Bakker, S de Groot and M Sciolla**;** *Irradiation of High Temperature Reactors Fuel Pebbles at VHTR in the HFR Petten.* Petten, The Netherlands: European Commission, Joint Research Centre, Institute for Energy, 2004.

22. D Petti G Miller and JT Maki**;** *Development of Improved Models and Designs For Coated-Particle Gas Reactors Fuels.* s.l.: Idaho National Engineering and Environment Laboratory, 2004.

23. A Cottrel**;** *An introduction to Metallurgy, 2nd edition.* London: Edward Arnold, 1982.

24. SH Avner**;** *Introduction to Physical Metallurgy, 2nd edition.* Tokyo: McGraw-Hill, 1983. ISBN 0-07-085018-6.

25. SJ Heyes**;** Chemistry Lectures. *Structure Of Simple Inrganic Solids.* [Online] Oxford University, 1999. [Cited: 13 March 2009.] http://www.chem.ox.ac.uk/icl/heyes/structure_of_solids/lecture1/lec1.html #anchor4.

26. WJ Weber, LM Wang and N Yu**;** *Irradition-induced crystalline-to-amorphous phase Transition in Alpha-SiC.* New Mexico: Eservier, 1996, Vol. NIMB. 116(1996)322-326.

27. L Calcagno**;***Crystallisation Mechanism Of Amorphous Silicon Carbide.* Catania, Italy: Elservier, 2001.

28. Jackson, KA**;** *Kintic Processes:Crystal Growth, Diffussion and Phase Transition In Materials.* Darmstadt: Wiley-VCH Verlag GmBH & Co.KGaA, 2004.

29. LL Snead, D Petti, T Nozawa, Y Katoh, T Byun and S Kondo**;** *Handbook of SiC Properties For Fuel Performance Modelling.* Idaho: Science Direct, 2007.

30. SJ Garrett; Crystal Structure Of Elements. *CEM 924.* [Online] Michigan State University, 9 May 2001. [Cited: 13 March 2009.] http://www.cem.msu.edu/~cem924sg/PeriodicTable.html.

31. WJ Weber, W Jiang and S Thevuthasan; *Accumulation, dynamic annealing and thermal recovery of ion-beam induced disorder in Silicon Carbide.* Richland: elsevier, 2001.

32. WJ Weber; *Structure and properties of ion-beam-modified (6H)Silicon Carbide.* Richland,USA: Science Direct, 1998.

33. GS Was**;** *Fundamentals of Radiation Material Science.* Ann Arbor: Springer-Verlag, 2007.

34. YUM Tairo, and VF Tsvetkov; Thermal properties of SiC. *http://www.ioffe.rssi.ru/SVA/NSM/Semicond/SiC/thermal.html#Phase%20 diagram.* [Online] mytrix, 1988. [Cited: 18 April 2009.] http://www.ioffe.rssi.ru/SVA/NSM/Semicond/SiC/thermal.html#Phase%20diagram.

35. DE Caro, JA Donell and BM Spicer; *Modern Physics: An Introduction to Atomic And Nuclear Physics.* Tokyo: McGraw-Hill, 1989.

36. R Gautreau and W Savin**;** *Theory and Problems o Modern Physics, Schaum outline series.* Toronto: McGraw-Hill, 1978. ISBN 0-07-023062-5.

37. CC Lin**;** *Radiochemistry in Nuclear Power Reactors.* Washington DC : National Academy Press, 1996.

38. K Minato,T Ogawa, S kashimura, K Fukuda, M Shimizu, Y Tayama and I Takahashi**;** *Fission Product Palladium-Silicon Carbide Interaction In HTGR Fuel Particles.* Ibaraki-ken: North Holland, 1990.

39. K Minato, K Fukuda, A Ishikawa and N Mita**;** *Advance Coatings for HTGR fuel particles against corrosion of SiC Layer.* Ibaraki-ken, Japan: Elservier, 1997.

40. K Minato, T Ogawa, S Kashimura and K Fukuda; *Metallic Impurities-Silicon carbide interaction in HTGR Fuel Particles.* Ibaraki-ken, Japan: North Holland, 1990.

41. K Minato, T Ogawa, S Kshimura, K Fukuda, I Takahashi, M Shimizu and Y Toyama; *Carbon Monoxide-Silicon Carbide Interaction in HTGR Fuel Particle.* Ibaraki-ken, Japan: Chapman and Hall Ltd, 1991.

42. Benyagoub**;** *Irradiation effects induced in silicon carbide by low and high energy ions.* Caen Cedex: Science Direct, 2008, Vol. Nuclear Instrumentation And Methods in Physics Research. B266(2008)2766-2771.

43. RJ Lauf, TB Lindermer and RL Pearson**;** *Out-Of-Reactor Studies Of Fission Product-Silicon carbide Interaction In HTGR Fuel Particles.* Amsterdam: North Holland, 1983.

44. GK Miller, DA Petti, JT Maki and DL Knudson**;** *An evaluation of the effects of SiC layer thinning on failure of TRISO-coated fuel particles.* Idaho: Science Direct, 2006, Vol. Journal of Nuclear Materials. 355(2006)150-162.

45. I Golubev and I Kadarmetov**;** *Current Status Of development Of Coated Particle Performance Code Golt.* Johannesburg: HTR2006, 2006. 3rd International Topical Meeting On High Temeperature Reactor Technology.

46. H Jiang-Feng, Z Xie-Rong, L He-Ju, X Xi-Bo and F Ye-Wei**;** *Influence of Preparation Temperature on the phase microstructure and anti-oxidation property of SiC coating for C/C composites.***.** Shnnxi: Science Direct, 2004, Vol. Carbon. 42(2004)1517-1521.

47. GK Miller and RG Bennet**;** *Analytical Solutions For Stress In TRISO-Coated Particle.* Idaho: Elsevier, 1993.

48. S Gosse**;** *High Temperature Interaction Between UO2 and Carbon: Application To TRISO Particle For Very High Temperature Reactors.* Washington: HTR, 2008. 4th International Topical Meeting On High Temeperature Reactor Technology.

49. D Gosset, M Dolle and D Simeone, G Baldinozzi, L Thome**;** *Structural Evolution of zirconium carbide under ion irradiation.* Orsay: Elsevier, 2007.

50. IAEA**.** *Fuel Performance and Fission Product Behaviour In Gas cooled Reactors-TECDOC 978.* Vienna: IAEA, 1997.

51. J Conrad**;** *Irradiation effects in alpha-SiC studied via RBS-C, Raman-Scattering and Surface Profiling.* Amsterdam: Science Direct, 1996.

52. SG Prussin, DR Orlander, WK Lau and L Hansson**;** *Release of Fission Products (Xe,I,Te,Cs,Mo and Tc)From Polyscrytalline UO_2.* Berkerly: North Holland, Amsterdam, 1988. 154(1988)25-37.

53. F Gelbard**;** *Analytical Modelling of Fission Product Release by Diffusion from Multicoated Fuel Particles.* Carlifonia: Sandia National Laboratory, 2003. Analytical.

54. NM Ghonien; *Helium Migration and its influence on Cavity Formation in Irradiated Materials.* Los Angeles: Elservier, 1993.

55. R Kemp, G Cottrell and KDH Bhadeshia**;** *Classical Thermodynamic approach to Void nucleation in irradiated materials.* oxfordshire: WSManey & Son Ltd, 2006.

56. GK Miller, DA Petti and JT Maki**;** *Consideration Of The Effects Of Partial Debonding Of IPyC And Particle Asphericity On TRISO-coated Fuel Behaviour.***.** Idaho: Elsevier, 2004.

57. K Sawa, J Sumita and S Suzuki; *Development of a Coated Fuel Particle Failure Model Under High Burnup Irradiation.* 9, Tokai, Japan: Journal Of Nuclear Scienceand Technology, 1996, Vol. 33.

58. VI Dubinko, AA Turkin, DI Vainshtein and HW den Hartog**;** *Evolution of defect structure and explosive decomposition of NaCl under electron irradiation.* Groningen: University Of Groningen, 2000.

59. J Rest, GL Hofman, II Konovalov and AA Maslov**;** *Experimental and Calculated Swelling Behaviour of U-10 wt%Mo Under Low Irradiation Temperature.* [Electronic] Illinois: Argonne National Laboratory.

60. R Takahashi, M Toyara, S Maruki, H Ueda and T Yamamoto**;** *Investigation of Morphology And Impurity Of Nuclear Graphite And Leaching Mechanism of Carbon-14.* Tokyo: Toshiba Corporation, 2007.

61. E Oliviero, MF Beaufort, F Pailloux and, JF Barbot**;** *Damage formation in high energy helium implanted 4H-SiC.***.** Marie te Pirre Currie: Science Direct, 2004.

62. T Nozawa, LL Snead, Y Katoh and JH Miller**;** *Shear Properties at PyC/SiC interface of a TRISO-coating.* Oakridge: Science Direct, 2007, Vol. Jounal of nuclear materials. 371(2007)304-313.

63. T Nozawa, LL Snead, Y Katoh, JH Miller and E Lara-Curzio**;** *Determining the Shear properties of the PyC/SiC interface for a model of TRISO fuel.***.** Oak Ridge: Elsevier, 2006, Vol. Journal of nuclear materials. 350(2006)182-194.

64. **NN**R**;** *Basic Licensing Requirement For the Pebble Bed Modular Reactor*. s.l.: NNR, 2009.

65. JR Parrington, HD Knox, SL Breneman, EM Baum and F Feiner**;** *Chart of the nuclide, 5th edition.* s.l.: Knoll Atomic Power Laboratory Naval Reactors, US Department of Energy, 1996.

66. K Matsukawa**;** *Gettering mechanism of transition metals in silicon calculated from first principles.* Hyogo, Japan: Elsevier, 2006.

67. M Sheoran, A Upadhayaya and A Rohatgi**;** *Bulk lifetime and efficiency enhancement to gettering and hydrogenation of defects during cast multicrystalline silicon solar cell fabrication.* Atlanta : Elsevier, 2008.

68. K Verfondern, H Nabielek and J Kendall**;** *Coated Particle Fuel For High Temperature Gas Cooled Reactors.* Julich, Germany: Nuclear Engineering Technology, 2007, Vol. 39 No 5.

69. Parliament, RSA**.** Parliament Speeches. *Parliament.* [Online] 20 October 2004. [Cited: 18 February 2009.] http://www.info.gov.za/speeches/2004/04102109151001.htm.

70. G.K Miller and RG Bennet**;** *Analytical Solutions for Stress in TRISO-coated particles.* Idaho: North Holland, 1993.

71. GK Miller, D Petti, DJ Varacalle and JT Maki**;** *Consideration Of The Effects On Fuel Particle Behaviour From Shrinkage Cracks In The Inner Pyrocarbon Layer.* Idaho: Elsevier, 2001.

72. GK Miller D Petti, DJ Varacalle and JT Maki**;** *Current capabilities of the fuel performance modelling code Parfume.*

73. W Mannhart and D Schmidt**;** *Measurement of the Si-28(n,p), Si-29(n,p) and Si-30(n,alpha)Cross Sections between 6.9 and 14.0MeV.* Supplement 2, Baunschweig, Germany: Nuclear Science And Technology, 2002.

74. Information, South African Government**.** http://www.info.gov.za/asgisa/asgisa.htm. *http://www.info.gov.za/asgisa/asgisa.htm.* [Online] South African

Government Information, 2004. [Cited: 18 February 2007.] http://www.info.gov.za/asgisa/asgisa.htm.

75. J, B Huang, K Tsuchiya, M Konashi and M Yamawaki**;** *Thermodynamic Analysis of chemical States Of fission Products In Uranium-Zirconium Hydride Fuel.* Hgashi-Ibaraki-gun: Elservier, 2001.

76. I Golubev and I Kadarmetov**;** *Current Status Of Development Of Coated Particle Performance Code GOLT.* Johannesburg: International Topical Meetings On High Temperature Reactor Technology, 2006. HTR2006.

77. M Dombsky; *Release of Al from SiC targets used for radioactive ion beam production.* Vancouver: Science Direct, 2007.

78. DME; *Government Gazette No 31954, 27 February 2009.* Pretoria: DME, 2009.

79. L I Deych, A Yamilov and AA Lisyansky**;** *Effect Of Resonant Tunneling in electromagnetic wave propagation through apolariton gap***.** 17, New York: American Physical Society, 1998, Vol. 59. S0163-1829(99)03418-9.

80 B Pershagen; *Light Water Reactor Safety*. Oxford: Pergamon Press, 1989, ISBN 0-08-035915-9

81 R Conrad, R Van Ulft and L Coutinho; *Irradiation Progress Report no. 10 HFR cycle: 93.01, Project D 138.06, HFR-K5*: Petten, Commission of the European Communities Joint Research Centre, Institute for Advanced Materials, Petten site, HFR Division

82 I Golubev, I Kadarmetov, V Makarov; *Mathematical Model And Computer Code For Coated Particles Performance At Normal Operating Conditions,*HTR 2002, Petten, The Netherlands, April 22-24, 2002

83 E Proksch, A Striggl, H Nabielek; *Production of Carbon Monoxide During Burn-up Of UO_2 Kerneled HTR Fuel Particles.* Journal of Nuclear Material 107. North Horland Publishing Company.